Article

Immunity

Natural Parasite Exposure Induces Protective Human Anti-Malarial Antibodies

Graphical Abstract

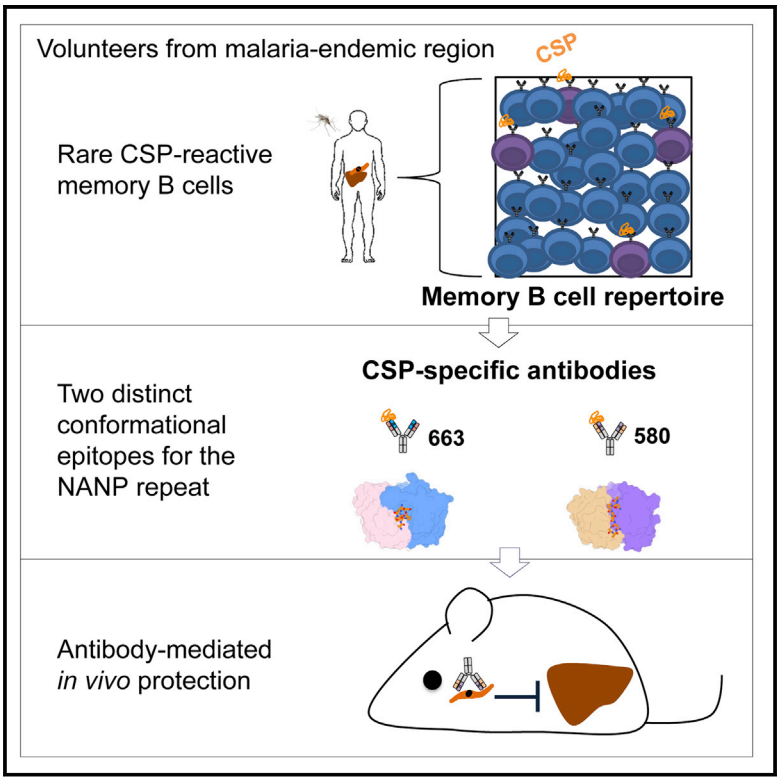

Authors

Gianna Triller, Stephen W. Scally, Giulia Costa, ..., Elena A. Levashina, Jean-Philippe Julien, Hedda Wardemann

Correspondence

jean-philippe.julien@sickkids.ca (J.-P.J.), h.wardemann@dkfz-heidelberg.de (H.W.)

In Brief

CSP is the target of protective antibodies against the malaria parasite *Plasmodium falciparum* (*Pf*). Here, Triller and Scally et al. identified potent *Pf*-inhibitory human anti-CSP memory B cell antibodies induced by natural exposure and unveiled the molecular details of antigen binding to two protective CSP repeat epitopes.

Highlights

- Long-term natural *Pf* exposure induces weak human CSP-memory B cell responses
- Anti-CSP memory B cell antibodies protect from *Pf* transmission and development
- *Pf*-inhibitory antibodies can recognize two distinct CSP NANP conformations
- NANP repeat recognition is largely mediated by germline-encoded residues

Triller et al., 2017, Immunity *47*, 1197–1209
December 19, 2017
https://doi.org/10.1016/j.immuni.2017.11.007

CellPress

Immunity
Article

Natural Parasite Exposure Induces Protective Human Anti-Malarial Antibodies

Gianna Triller,[1,12] Stephen W. Scally,[2,12] Giulia Costa,[3] Maria Pissarev,[3] Cornelia Kreschel,[3] Alexandre Bosch,[2] Eric Marois,[4] Brandon K. Sack,[5] Rajagopal Murugan,[1] Ahmed M. Salman,[6,7] Chris J. Janse,[7] Shahid M. Khan,[7] Stefan H.I. Kappe,[5] Ayola A. Adegnika,[8,9,10] Benjamin Mordmüller,[9] Elena A. Levashina,[3] Jean-Philippe Julien,[2,11,*] and Hedda Wardemann[1,13,*]

[1]B Cell Immunology, German Cancer Research Center, Heidelberg, 69120, Germany
[2]Program in Molecular Medicine, The Hospital for Sick Children Research Institute, Toronto, ON M5G 1X8, Canada
[3]Vector Biology Unit, Max Planck Institute for Infection Biology, Berlin, 10117, Germany
[4]UPR9022 CNRS, U963 Inserm, Université de Strasbourg, Strasbourg, 67000, France
[5]Seattle Biomedical Research Institute, Seattle, WA 98109, USA
[6]The Jenner Institute, Nuffield Department of Medicine, University of Oxford, Oxford, OX3 7DQ, UK
[7]Leiden Malaria Research Group, Parasitology, Center of Infectious Diseases, Leiden University Medical Center, Leiden, 2333 ZA, The Netherlands
[8]Centre de Recherches Médicales de Lambaréné, Lambaréné, 242, Gabon
[9]Institute of Tropical Medicine and German Center for Infection Research, partner site Tübingen, University of Tübingen, Tübingen, 72074, Germany
[10]Leiden University Medical Centre (LUMC), Leiden, 2333 ZA, The Netherlands
[11]Departments of Biochemistry and Immunology, University of Toronto, ON M5G 0A4, Canada
[12]These authors contributed equally
[13]Lead contact
*Correspondence: jean-philippe.julien@sickkids.ca (J.-P.J.), h.wardemann@dkfz-heidelberg.de (H.W.)
https://doi.org/10.1016/j.immuni.2017.11.007

SUMMARY

Antibodies against the NANP repeat of circumsporozoite protein (CSP), the major surface antigen of *Plasmodium falciparum* (*Pf*) sporozoites, can protect from malaria in animal models but protective humoral immunity is difficult to induce in humans. Here we cloned and characterized rare affinity-matured human NANP-reactive memory B cell antibodies elicited by natural *Pf* exposure that potently inhibited parasite transmission and development *in vivo*. We unveiled the molecular details of antibody binding to two distinct protective epitopes within the NANP repeat. NANP repeat recognition was largely mediated by germline encoded and immunoglobulin (Ig) heavy-chain complementarity determining region 3 (HCDR3) residues, whereas affinity maturation contributed predominantly to stabilizing the antigen-binding site conformation. Combined, our findings illustrate the power of exploring human anti-CSP antibody responses to develop tools for malaria control in the mammalian and the mosquito vector and provide a molecular basis for the structure-based design of next-generation CSP malaria vaccines.

INTRODUCTION

Plasmodium falciparum (*Pf*) is a protozoan parasite with a complex life cycle that causes malaria, a severe and potentially fatal disease. *Pf* is transmitted to humans by infected female *Anopheles* mosquitoes, which inject small numbers of sporozoites into the skin during their blood meals. The infection is established within hours after the injected sporozoites migrate to the liver and invade hepatocytes. Upon further development, blood stage parasites are released from the infected hepatocytes and undergo successive rounds of multiplication in erythrocytes. The increase in blood stage parasitaemia causes disease symptoms and may lead to life-threatening complications without treatment. In endemic areas, immunity to *Pf* develops slowly after repeated infections but is rarely sterile (Bousema et al., 2014; Doolan et al., 2009; Langhorne et al., 2008; Struik and Riley, 2004). Therefore, a major goal in vaccine development remains to induce sterilizing immunity through anti-sporozoite antibodies and T cell responses. The target antigen of the most advanced *Pf* malaria subunit vaccine RTS,S is circumsporozoite protein (CSP), the major sporozoite surface protein (Aikawa et al., 1981; Cohen et al., 2010; Yoshida et al., 1980). *Pf* CSP consists of an N-terminal domain, a central region consisting predominantly of NANP repeats, which differs in length between individual *Pf* strains, and a C-terminal domain. CSP plays a critical role in the *Plasmodium* life cycle and is essential for parasite development in the mosquito vector and the mammalian host (Cerami et al., 1992; Frevert et al., 1993; Ménard et al., 1997; Sidjanski et al., 1997).

The B cell response to CSP targets predominantly the central NANP region. Antibodies against the NANP repeat can protect from *Plasmodium* infection in animal models and anti-CSP titers are associated with protection after RTS,S immunization (Foquet et al., 2014; RTS,S Clinical Trials Partnership, 2015; Sumitani et al., 2013; White et al., 2013). However, RTS,S shows relatively low and short-lived efficacy, and serum antibody titers wane

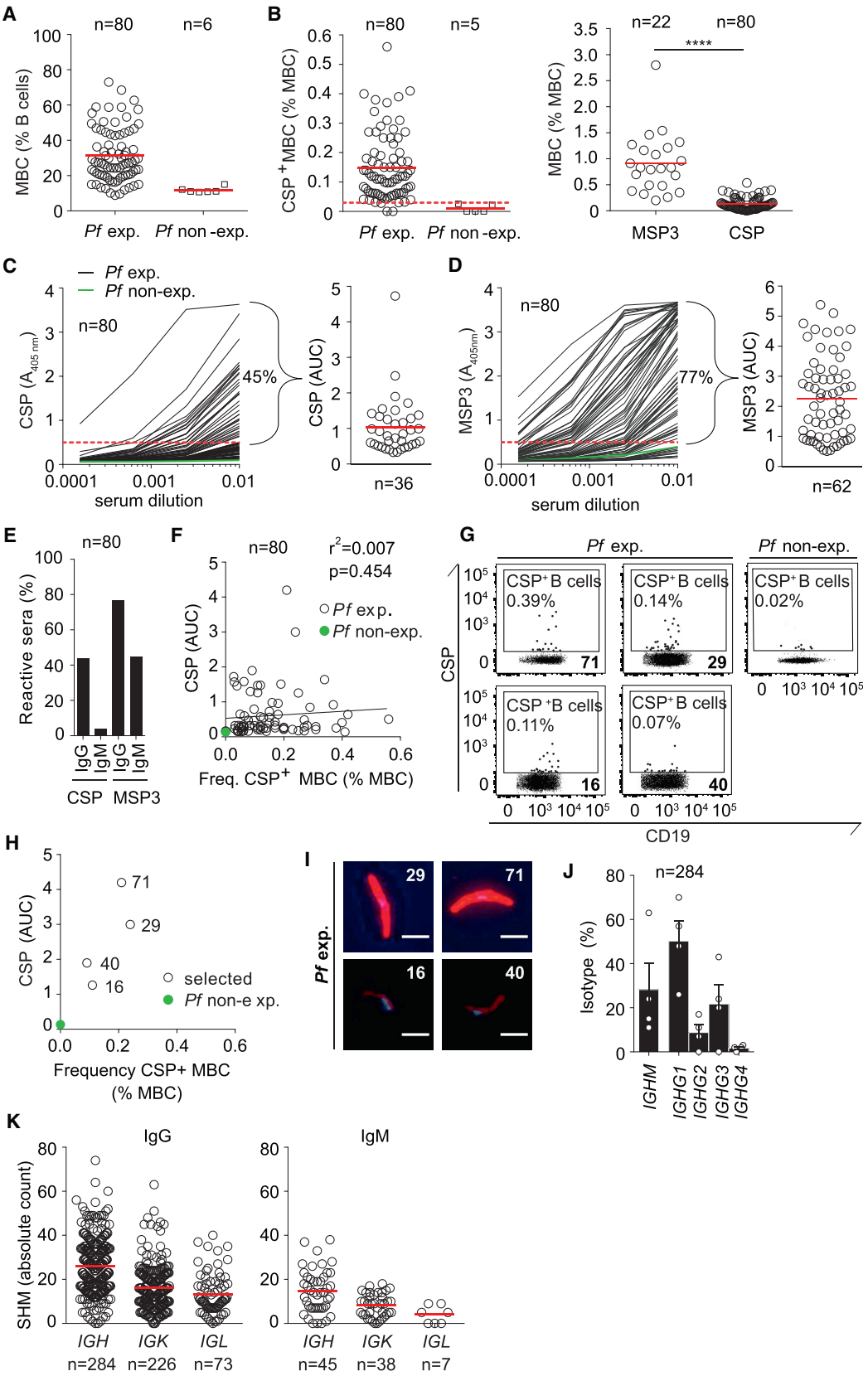

(legend on next page)

quickly in the absence of repeated natural *Pf* exposure suggesting that protective B cell memory against CSP may not form efficiently (Crompton et al., 2014; Langhorne et al., 2008; Offeddu et al., 2012; Portugal et al., 2013; Struik and Riley, 2004). A deeper understanding of the molecular and functional characteristics of human memory B cell antibodies can provide important insights into the development of protective antibody responses and facilitate the rational design of novel vaccination strategies as demonstrated for other pathogens (e.g. RSV [Boyington et al., 2013], HIV [Briney et al., 2016; Escolano et al., 2016; de Taeye et al., 2015; Tian et al., 2016]). Here, we used single-cell antibody cloning to determine the frequency and quality of human anti-CSP memory B cell antibodies that developed in response to natural *Pf* exposure and defined the structural basis of antigen recognition that underlies parasite inhibition.

RESULTS

Weak anti-CSP Memory B Cell Responses Develop after Long-Term Natural *Pf* Exposure

To identify and isolate CSP-reactive memory B cells, we collected blood samples for the isolation of mononuclear cells from 80 healthy adults living in the malaria-endemic area of Lambaréné, Gabon (Figure 1A). Although the time-point of the last infection was unknown, we assume that all of these donors had a history of repeated *Pf* exposure. African donors showed higher frequencies of total memory B cells compared to *Pf* non-exposed European donors, likely reflecting differences in the overall immune status and degree of exposure to pathogens (mean = 31.2 ± SD = 15.1 and mean = 11.8 ± SD = 1.6, respectively, Figure 1A). Using fluorescently-labelled CSP and MSP3, a representative blood stage antigen, we determined the frequency of CSP- and MSP3-reactive memory B cells in flow cytometric analyses. We defined memory B cells as CSP-reactive $CD19^+CD27^+IgG^+$, $CD19^+CD27^-IgG^+$, or $CD19^+CD27^+IgG^-$ (Figure S1A). In the absence of acute *Pf* exposure and high frequencies of circulating plasmablasts, a small fraction of these cells might express the plasmablast marker CD38 (Keitany et al., 2016). CSP-reactive memory B cells above background (European donors with no history of *Pf* exposure) were detected in 77/80 African donors albeit at relatively low frequency (mean = 0.15 ± SD = 0.1, range 0.03%–0.56%, Figure 1B) compared to the frequency of memory B cells against MSP3 (mean = 0.9 ± 0.57, range = 0.2% - 2.8%. Muellenbeck et al., 2013). Overall weak anti-CSP responses compared to MSP3 were also observed at serum antibody level (Figures 1C and 1D). Only 45% and 4% of donors exhibited circulating IgG and IgM anti-CSP antibodies, respectively, independent of the frequency of anti-CSP memory B cells (Figures 1E and 1F).

To determine the molecular features of anti-CSP memory B cell antibodies induced by natural *Pf* exposure, we selected four donors with high (donors 71, 29) or intermediate (donors 40, 16) anti-CSP serum titers for the flow cytometric isolation of single CSP-reactive memory B cells and subsequent Ig gene amplification and sequencing (Figures 1G and 1H and S1A). When used in immunofluorescence assays (IFA), only sera from donors with high anti-CSP serum titers showed strong IgG sporozoite reactivity (Figure 1I). Ig gene sequence analysis determined that on average almost 30% of the CSP-reactive memory B cells were IgM (range 11%–63%). As expected, these antibodies had been cloned exclusively from cells that lacked surface IgG expression demonstrating the validity of our gating strategy and assumption that CSP-reactive IgG^- memory B cells are non-switched IgM expressing cells. Overall, IgG was the most prominent isotype detected in three donors with a strong contribution of IgG1 and IgG3, typically enriched in anti-CSP responses, whereas IgM was dominant only in donor 29 (Figures 1J and S1B) (Ikpa and Adebambo, 2011; John et al., 2008; Krishnamurty et al., 2016; Noland et al., 2015). Independent of the isotype, the vast majority of *IGH*, *IGK*, and *IGL* genes were somatically mutated indicating that the response in all donors involved IgG^+ as well as IgM^+ memory B cells (Figures 1K and S1C). This is in line with a recently reported role for IgM^+ memory B cells in *P. chabaudi* infection in a rodent model (Krishnamurty et al., 2016). Shared somatic hypermutations (SHM) in different antibody genes from individual donors indicated that these cells

Figure 1. Characterization of anti-CSP Memory B Cells

(A) Frequency of peripheral blood MBCs in healthy *Pf* exposed (*Pf* exp.) African and in non-exposed (*Pf* non-exp.) European donors as determined by flow cytometry.

(B) Frequency of CSP-reactive MBCs in the same samples as in (A) (left). Frequency of MSP3-reactive MBCs in a representative subset of samples compared to the frequency of CSP-reactive MBCs after normalization to the respective non-exposed European donors (right).

(C) Representative anti-CSP IgG ELISA (left) for sera from the same *Pf* exposed donors (left, black lines) and one non-exposed donor (left, green line) as in (A) and corresponding area under curve (AUC) values for positive sera (right). Percentage of CSP-reactive sera is indicated.

(D) Representative anti-MSP3 IgG ELISA (left) and corresponding AUC values for anti-MSP3 IgG positive sera (right) for the same donors as in (C). Percentage of positive sera is indicated.

(E) Percentage of anti-CSP and anti-MSP3 IgG or IgM positive sera from *Pf* exposed donors identified in (C and D).

(F) Linear regression between percentage of CSP-reactive MBCs (B) and anti-CSP serum IgG ELISA AUC (C) from *Pf* exposed donors (open circles) and one representative non-exposed control (green circle).

(G) Sort gates for CSP-reactive B cells in four *Pf* exp. and one non-exp. donor after pre-gating as in S1A. Cell frequencies for the gated populations are indicated. Bold numbers indicate donor IDs.

(H) Correlation between the frequency of CSP-reactive MBCs (B) and anti-CSP IgG ELISA reactivity (AUC) (C) for the same donors as in (G).

(I) Representative serum IgG immunofluorescence reactivity (red) with *Pf* sporozoites and DAPI-stained *Pf* sporozoite nuclei (blue) (bars, 5 μm) for the same donors as in (G and H).

(J) Mean *IGHM* and *IGHG1-4* isotype distribution in the same donors as in (G)–(I) (circles) and for all donors pooled (bars). Error bars show SD.

(K) *IGHV*, *IGKV*, and *IGLV* SHM base pair counts for all donors pooled.

n indicates the number of donors (A, B, and F) and the number of tested sera (C–E), or the number of Ig gene sequences (J and K) that were analyzed. Solid red lines in (A–D and K) show arithmetic means. Dashed lines in (B–D) depict threshold for CSP and MSP3 reactivity. Data are representative of two (A, B, G, and I) or three independent experiments (C and D). Data in (B) were analyzed using Mann-Whitney test, ****$p < 0.0001$. See also Table S1.

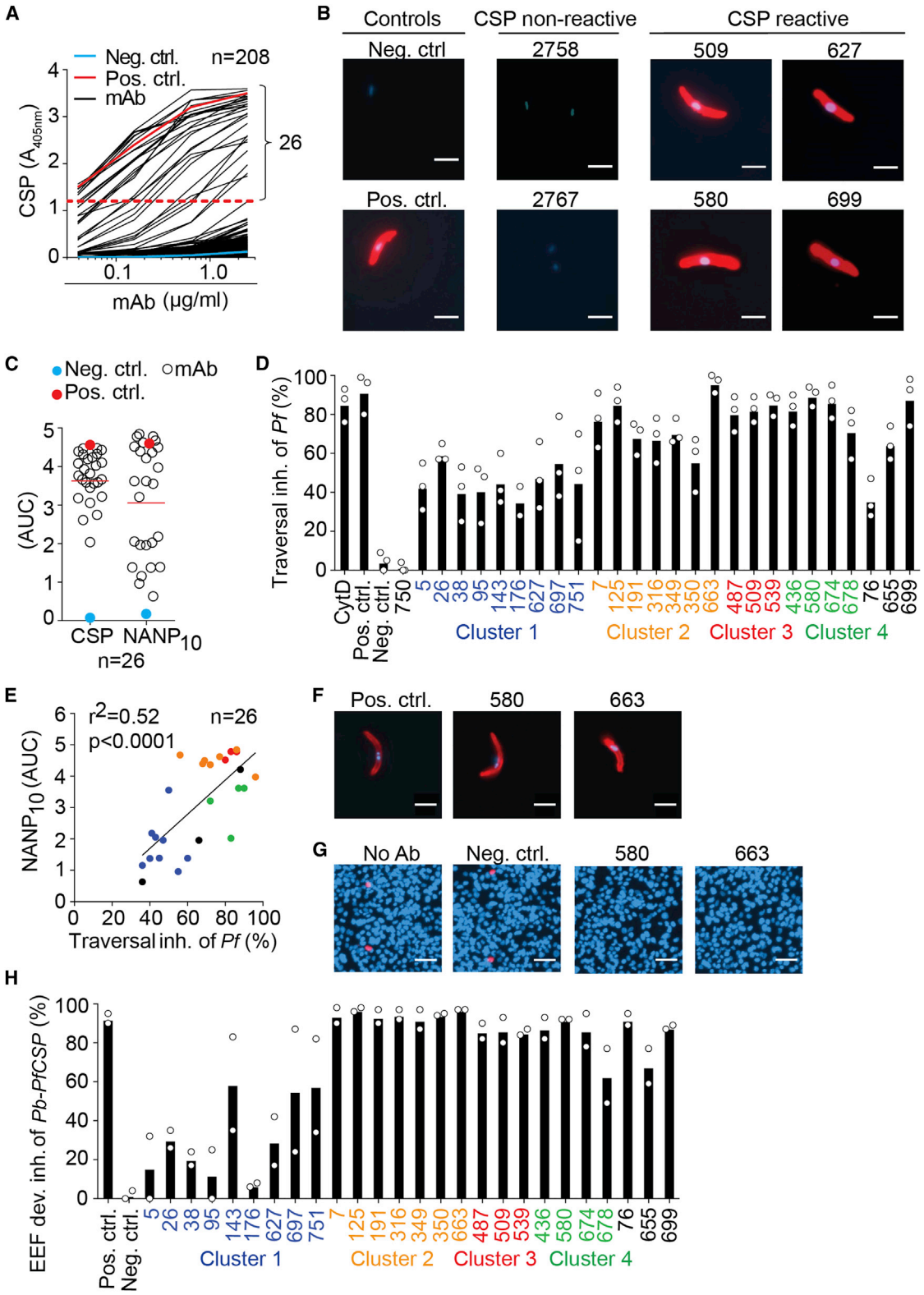

Figure 2. Functional *In Vitro* Characterization of CSP-Reactive MBC Antibodies

(A) Representative CSP-ELISA reactivity of recombinant monoclonal antibodies (mAb) (black lines) and positive (pos. ctrl., red line) and negative (neg. ctrl., blue line) control antibodies. Dashed red line depicts threshold for CSP reactivity.

(B) Representative mAb immunofluorescence reactivity (red) with *Pf* sporozoites and DAPI-stained *Pf* sporozoite nuclei (blue) (bars, 5 μm).

(legend continued on next page)

had originated from a common ancestor cell and underwent clonal expansion and substantial diversification presumably during germinal center reactions. Such clonally related cell clusters of different sizes were identified in all donors and varied in their degree of mutational diversity among the members (Figures S1D and S1E). In donor 71, clonally related cells from 6/13 clusters were also isolated from a blood sample two years later, demonstrating that the clusters were stable over this time (Table S1). All of these clusters had undergone class-switching to IgG1, IgG2, or IgG3 subtypes, and the largest cluster comprised IgG1 and IgG3 cells.

Thus, natural *Pf* exposure induces weak anti-CSP serum and memory B cell responses but individual IgG memory B cell clones persist and diversify over years.

Anti-CSP Memory B Cell Antibodies Recognize the Central NANP Repeat and Inhibit Sporozoite Traversal of Hepatocytes

To assess the quality of the anti-CSP response, we cloned and expressed the Ig genes of 208 memory B cells from the four selected donors and measured the reactivity of the recombinant monoclonal antibodies by enzyme-linked immunosorbent assay (ELISA). Only 27 antibodies showed detectable CSP-ELISA and whole sporozoite IFA reactivity at the concentrations tested (Figures 2A and 2B). These antibodies, cloned exclusively from the donors with the highest anti-CSP serum titers, carried substantial numbers of somatic mutations, and were either IgM or class-switched (Table S2). With one exception, these antibodies were CSP-specific and lacked cross-reactivity with unrelated antigens (Figure S1F and Table S2). The majority of antibodies recognized the NANP repeat, a well-known B cell epitope and target of protective antibodies (Figure 2C) (Dups et al., 2014). The repetitive nature of this region in the full-length CSP might have contributed to the avidity-based isolation of memory B cells expressing antibodies with low or undetectable CSP-ELISA and IFA reactivity. This biological interpretation is supported by the results of an independent study of a controlled human malaria infection trial using the same CSP-based isolation strategy. In this study, only few monoclonal antibodies with high CSP-ELISA reactivity were cloned from memory B cells obtained after only one *Pf* infection, whereas the majority lacked detectable CSP-ELISA reactivity. However, after a second or third *Pf* infection the majority of cloned antibodies were CSP-ELISA reactive and only a few showed no detectable CSP-reactivity in ELISA (Murugan et al., G.T., C.K., G.C., E. A.L., B.M., and H.W., unpublished). We next examined the inhibitory activity of the cloned antibodies. With one exception, all (26/27) Pf CSP-reactive antibodies inhibited sporozoite traversal of hepatocytes *in vitro* (Figure 2D and Table S2). The degree of inhibition correlated with the NANP repeat ELISA reactivity and was similar for closely related antibodies within individual clusters (Figure 2E). Thus, antibodies derived from anti-CSP memory B cells induced by natural parasite exposure recognize predominantly the NANP repeat and block hepatocyte traversal of *Pf* sporozoites *in vitro*.

Anti-CSP Memory B Cell Antibodies Block Hepatocyte Infection

To determine whether the anti-CSP antibodies also inhibited hepatocyte infection and subsequent sporozoite development into exoerythrocytic forms (EEF), we generated a chimeric line (*Pb-PfCSP*) of the rodent *P. berghei* (*Pb*) parasite in which the endogenous *Pb CSP* gene was replaced with the full-length *Pf CSP* gene by homologous recombination (Figure S2). *Pb-PfCSP* developed equal sporozoite numbers in infected mosquitoes compared to the parental *Pb* line and showed similar *in vitro* infectivity based on EEF development in hepatocyte lines and *in vivo* infectivity in wild-type mice (Figures S2F–S2H). All 26 *Pf* inhibitory antibodies recognized *Pb-PfCSP* sporozoites and inhibited their further development into EEF (Figures 2F–2H) comparable to their inhibition of *Pf* cell traversal. Antibodies 125 and 663, two clonally related mutated IgG antibodies from donor 71, and antibody 580, a mutated IgM antibody cloned from a cluster of donor 29 (Table S2), showed the highest inhibitory activity (Figure S3A). These findings validate the use of the chimeric *Pb* line to assess the infection blocking activity of our antibodies and identified the most potent antibodies for further functional analyses.

NANP-Reactive Memory B Cell Antibodies Inhibit Malaria Transmission and Protect from Malaria Infection

We tested whether exposure of sporozoites to anti-CSP antibodies prior to transmission from the mosquito to the mammalian host might impair sporozoite infectivity (Sumitani et al., 2013; Yoshida and Watanabe, 2006). For this purpose, we generated a transgenic *Anopheles coluzzii* mosquito line (*Aapp::125*) expressing a FLAG-tagged single-chain Fv fragment of antibody 125 in their salivary glands and infected them with *Pb-PfCSP* (Figures S3B–S3D) (Sumitani et al., 2013; Yoshida and Watanabe, 2006). *Pb-PfCSP* sporozoites were isolated at normal numbers from the salivary glands of single-chain Fv-expressing *Aapp::125* compared to wild-type mosquitoes but were impaired in their development into EEF *in vitro* (Figure S3E). To test whether the antibody fragment could also block transmission *in vivo*, we allowed *Pb-PfCSP*-infected *Aapp::125* and *Pb-PfCSP*-infected wild-type mosquitoes to blood-feed on

(C) ELISA AUC values for CSP and $NANP_{10}$ reactivity of CSP-reactive mAb. Solid red line shows arithmetic means.
(D) *Pf* hepatocyte traversal inhibition (inh.) by recombinant MBC mAb and control mAbs.
(E) *Pf* hepatocyte traversal inhibition (inh.) versus $NANP_{10}$ ELISA AUC reactivity.
(F) Representative anti-CSP immunofluorescence reactivity (red) and DAPI-stained *Pb-PfCSP* sporozoite nuclei (blue) (bars, 5 μm).
(G) Representative microscopy pictures of *Pb-PfCSP* EEF cultures.
(H) Inhibition of *Pb-PfCSP* EEF development (dev.) by recombinant MBC mAb and control mAbs. n in (A, C, and E) indicates absolute number of tested mAb. Bars in (D) and (H) depict mean of three independent experiments, white circles represent mean of two technical replicates in independent experiments. Positive control antibody, Cytochalasin D (CytD) and negative control antibody are shown. Colored labels in (D), (E), (H) indicate clonally related antibodies from the indicated MBC clusters, non-cluster antibodies are labeled in black. Data in (A) and (C) and in (B), (F), (G), and (H) are representative of three and two independent experiments, respectively. See also Figures S1 and S2 and Table S2.

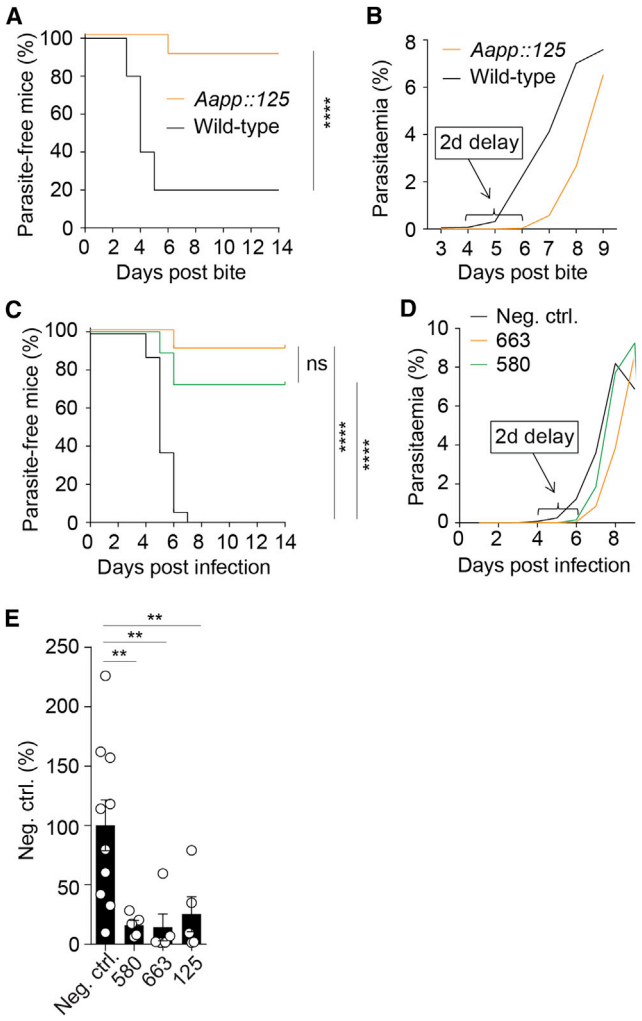

Figure 3. *In Vivo* Parasite Inhibitory Activity of CSP-Reactive MBC Antibodies

(A) Parasite-free mice after exposure to bites of *Pb-PfCSP*-infected wild-type (black line) or *Aapp::125* mosquitoes (orange line) (n = 10 per group).

(B) Mean parasitaemia in infected mice after exposure to bites of *Pb-PfCSP*-infected wild-type or *Aapp::125* mosquitoes as in (A).

(C) Parasite-free mice after passive immunization with the indicated antibodies before s.c. infection with *Pb-PfCSP* sporozoites (580, green, n = 6; 663, orange, n = 7; negative control, black, n = 5 individual mice for every experiment).

(D) Mean parasitaemia in infected mice after passive immunization with the indicated antibodies before s.c. infection with *Pb-PfCSP* sporozoites as in (C).

(E) Bioluminescence analysis of FRG-huHep mice challenged with bites from 50 *PfGFP-luc* sporozoites-infected mosquitoes after passive immunization with the indicated antibodies (580, n = 5; 663, n = 5; 125, n = 5; negative control, n = 10 individual mice; circle, one mouse; bar, mean ± SEM). Parasite burden was determined after normalization to the mGO53 control group. 1-way ANOVA with Kruskal-Wallis **p < 0.001, F(4, 25) = 6.456. Data in (A) and (B) are from three independent experiments and were analyzed using Log-rank Mantel-Cox test, ****p < 0.0001. See also Figure S3.

healthy mice. Blood stage parasites were detected in only 10% of mice exposed to bites from infected *Aapp::125* mosquitoes, whereas 80% of mice exposed to infectious bites of wild-type mosquitoes developed parasitaemia (Figure 3A). Notably, the single mouse infected by bites of *Aapp::125* mosquitoes showed a 2-day delay in the development of blood-stage parasites suggesting a substantial reduction in liver infection (Figure 3B). Thus, expression of an anti-CSP single-chain Fv in the mosquito salivary glands efficiently blocked parasite transmission to the mammalian host and strongly inhibited parasite development in the single case when protection was not complete.

To determine whether the antibodies would also protect mice from *Plasmodium* infection after passive immunization, we administered antibody 663, the clonal relative of 125 with slightly better performance in the *in vitro* assays, and antibody 580 intraperitoneally (i.p.) one day prior to infection by subcutaneous (s.c.) injection of *Pb-PfCSP* sporozoites (Figures 3C and 3D). Passive immunization protected the majority of mice (91% and 72% for 663 and 580, respectively) from the development of blood stage parasites (Figure 3C). The few animals in which the antibodies did not fully control the infection, developed blood stage parasitemia with a 2-day delay compared to control mice (Figure 3D).

To further validate our findings *in vivo*, we extended our analyses to the humanized FRG-huHep mouse model, which supports the development of *Pf* liver stages and is used to determine antibody-mediated inhibition of liver infection by bioluminescence after infection with a transgenic *Pf* parasite expressing GFP and luciferase (Sack et al., 2017; Vaughan et al., 2012a, 2012b). Passive immunization with antibody 125, 663, or 580 one day before exposure to the bites of infected mosquitoes strongly reduced parasite burden at the peak of liver infection compared to control FRG-huHep mice (Figure 3E).

In summary, antibodies 125, 663, and 580 protected the majority of mice from *Plasmodium* infection and substantially reduced hepatocyte infection and/or sporozoite development in the few non-protected animals after passive immunization or if expressed as single-chain Fv in the mosquito salivary gland. Thus, the NANP-repeat-specific memory B cell antibodies are potent inhibitors of malaria transmission and protect from parasite infection.

Pf-Inhibitory Antibodies Recognize Two Distinct NANP Conformations

To establish how the antibodies recognized the NANP repeat, we structurally characterized 580- and 663-Fabs and their predicted germline ancestors (580-g and 663-g). Co-crystal structures of antibody with a $NANP_5$ repeat peptide could be determined for the 580-g-Fab and the 663-Fab to 1.6 Å and 3.15 Å resolution, respectively (Figure 4 and Table S3). We observed strong electron density for at least seven of 20 *Pf* $NANP_5$ repeat peptide residues in each structure, indicating that both antibodies bind to a conserved core repeat (Figures S4A and S4B).

The antibodies show major differences in their antigen-binding mode and recognize distinct conformations of the $NANP_5$ peptide. 580-g binds to an elongated conformation of the $NANP_5$ peptide using a shallow interface between the light (L)- and heavy (H)-chain (Figures 4A–4C). Four of the six 580-g complementary determining regions (CDRs) contact the peptide (with HCDR1 and HCDR2 contributing no interactions), culminating in 522 $Å^2$ of buried surface area (Table S4). Interactions are dominated by the HCDR3, centering on Arg100E that is stabilized by

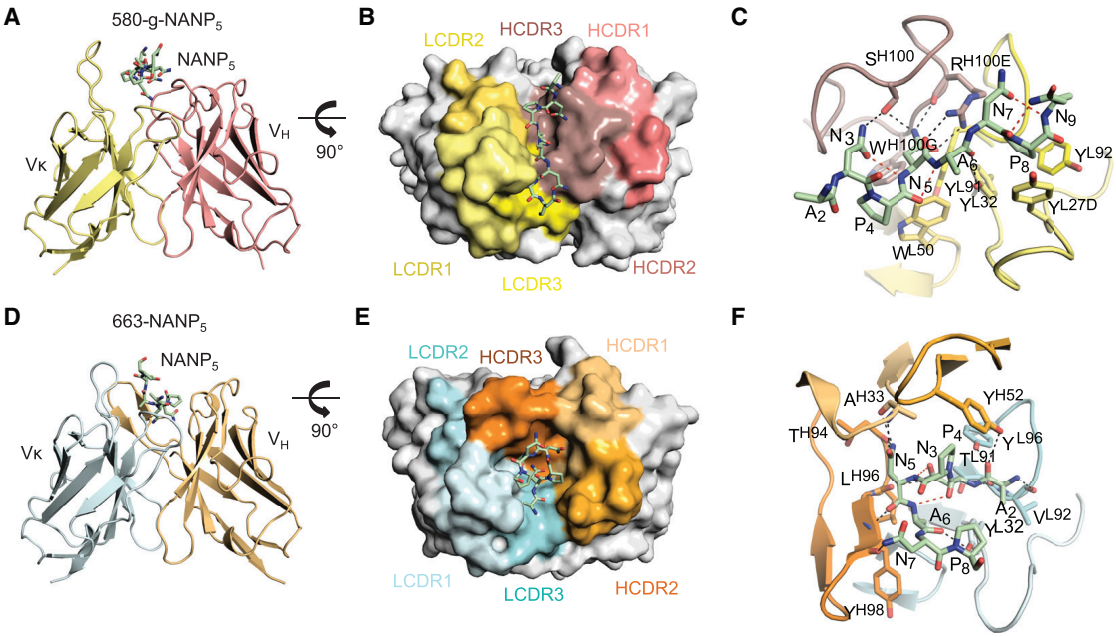

Figure 4. Crystal Structure and Interaction of $NANP_5$ in Complex with 580-Germline (g)-Fab and 663-Fab

(A) Cartoon representation of the 580-g Fab variable region. The 580-g L- and H-chains are colored in yellow and salmon, respectively. $NANP_5$ peptide is shown as green sticks.

(B) Surface representation of the 580-g paratope. The 580-g LCDR1, 2, and 3 regions are colored in shades of yellow. The 580-g HCDR1, 2, and 3 regions are colored in shades of salmon.

(C) Cartoon representation of the 580-g Fab variable region. Antibody residues that make H-bond contacts or form an aromatic cage surrounding prolines in the $NANP_5$ epitope are represented as sticks. Inter-chain H-bonds between the $NANP_5$ and the 580-g-Fab are shown as black dashes, while intra-chain H-bonds are shown as red dashes.

(D) Cartoon representation of the 663 Fab variable region. The 663 L- and H-chains are colored in cyan and orange, respectively. $NANP_5$ peptide is shown as green sticks.

(E) Surface representation of the 663 paratope. The 663 LCDR1, 2, and 3 regions are colored in shades of cyan. The 663 HCDR1, 2, and 3 regions are colored in shades of orange.

(F) Cartoon representation of the 663 Fab variable region. Antibody residues that provide H-bond contacts or form an aromatic cage surrounding prolines in the $NANP_5$ epitope are represented as sticks. Inter-chain H-bonds between the $NANP_5$ and the 663-Fab are shown as black dashes, while intra-chain H-bonds are shown as red dashes. See also Figure S4 and Tables S3–S5.

contacts to several residues of $NANP_5$ (Figure 4C and Table S4). Additionally, germline-encoded LCDR1 and LCDR3 Tyr residues L-27D, L-32, and L-92 stabilize binding through an aromatic cage around Pro8 (Figure 4C).

In contrast, 663 binds the $NANP_5$ peptide in a turn conformation via a deep cleft created by a radially oriented HCDR3 (Figures 4D–4F). All six 663 CDRs contribute to recognition of the peptide with a total of 582 $Å^2$ of buried surface area and the central NPNA hydrogen-bonds exclusively to main-chain atoms (Figure 4F and Table S5). The 663-bound peptide adopts a type I β-turn (Figure 5A and Table S6) in strong agreement with the previously determined crystal structure of an ANPNA peptide (superposing well over the NPNA cadence with an r.m.s.d. of 0.40 Å) (Ghasparian et al., 2006). In contrast, the 580-g-bound peptide adopts an elongated conformation (Figure 5B and Table S6) that forms an asx type II turn (with a r.m.s.d. of 0.29 Å over the NPNA cadence of the previously described NPNA crystal structure). Our peptide crystal structures are consistent with previous studies that have shown dynamic equilibrium between elongated and type I β-turn conformations with NANP peptides (Dyson et al., 1990).

Crystal packing positions two 663-Fab paratopes facing one another, with the C-terminus of one peptide and the N-terminus of the symmetry-related peptide separated by 11.8 Å (Figure S4C). Thus, it is conceivable that two 663-Fabs bind one $NANP_5$ peptide in our structure (Fisher et al., 2017). 663-Fab displayed a 10-fold higher affinity to CSP as compared to 580-Fab, with a much slower off-rate (Table S7), which is consistent with the more extensive antibody-antigen interactions observed in our co-crystal structure (Figures 4C and 4F, Tables S4 and S5).

To investigate the overall topology of 580 and 663 binding to full-length CSP, we performed size-exclusion chromatography small-angle X-ray scattering experiments (SEC-SAXS) on 580- and 663-Fab co-complexes with CSP from the 7G8 strain, which in contrast to NF54 contains only five NANP repeats. Co-complexes were incubated in a near stoichiometric molar ratio of antibody to CSP, prior to SEC-SAXS. 580- and 663-Fab CSP co-complexes (Figure S5) revealed that recognition of different core epitope conformations is also associated with binding in slightly different orientations (Figure 5C).

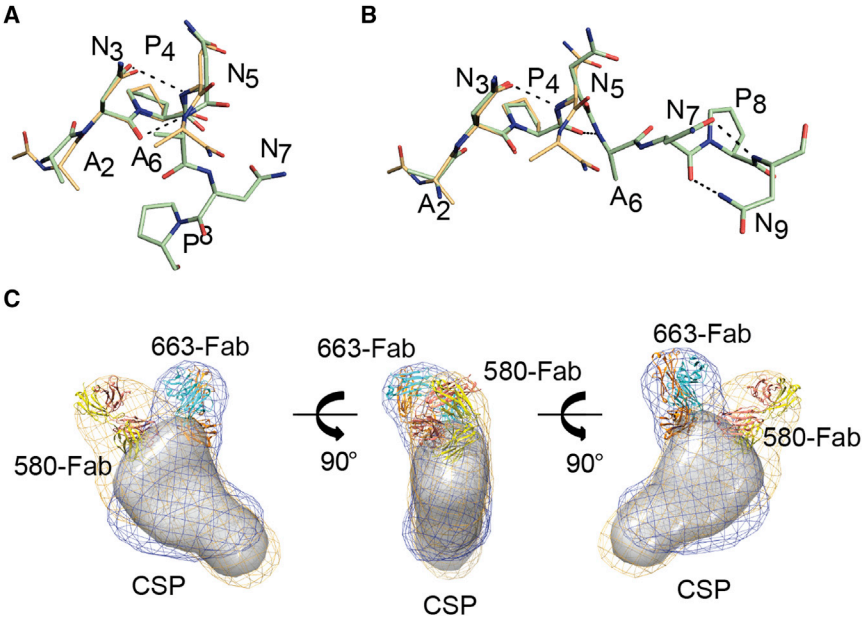

Figure 5. NANP Repeat Epitope Structures and Antibody Binding to Full-Length CSP

(A) Superposition of the 663 bound $NANP_5$ peptide with the previously described crystal structure of an ANPNA peptide colored in orange (Ghasparian et al., 2006). Intra-chain H-bonds are represented as black dashes.

(B) Superposition of the 580-g bound $NANP_5$ peptide with the previously described crystal structure of an ANPNA peptide colored in orange (Ghasparian et al., 2006). Intra-chain H-bonds are represented as black dashes.

(C) The 663-Fab and 580-g-Fab crystal structures docked into a SAXS envelope of 580-Fab-CSP and 663-Fab-CSP co-complexes. CSP alone is shown as surface and colored grey. See also Figure S5 and Tables S6 and S7.

Combined, our X-ray crystallography and SAXS studies show that the *Pf* inhibitory antibodies target two distinct CSP NANP-repeat configurations.

Somatic Mutations Stabilize the Conformation of the Paratopes

Next we explored the role of somatic mutations in generating potent NANP binders in response to natural parasite exposure. Antibodies 580 and 663 underwent a total of 39 and 58 SHM at nucleotide level, resulting in 27 and 32 amino acid exchanges, respectively (Figure S6). Expectedly, mutated 580 and 663 antibodies each bound with approximately 15-20- and 140-260-fold higher affinity to both the $NANP_5$ peptide and the recombinant CSP than their unmutated 580-g and 663-g counterparts, respectively (Figures 6A–6D and Table S7). Although CSP binding and *Pf* inhibition was reduced, it was not completely abrogated, indicating that germline-encoded residues play an important role in CSP binding (Figures 6E–6H and Table S7).

Indeed, analysis of unliganded 580-Fab and 663-g-Fab crystal structures revealed that mutated residues rarely generate additional contacts to the core *Pf* CSP epitope (Figures 7A and 7B). In 580, only a L-Lys30 to L-Arg30 mutation presumably leads to new contacts with the Pro4 carbonyl of the NANP epitope (Figure 7C). Core epitope recognition of the mutated antibodies is largely mediated by germline-encoded amino acids and HCDR3, whereas most affinity-matured residues do not contact the core peptide, raising the possibility of an expanded epitope in the context of full-length CSP (Figures 7A and 7B). Several mutations in 580 (Figure 7D) and 663 (Figures 7E and 7F) lead to stabilization of CDR conformations, rigidifying the antigen binding site while preserving a similar surface electrostatic potential (Figures S7A–S7D). Accordingly, the 663 unliganded structure reveals high conformational similarity in its CDRs compared to the $NANP_5$-bound structure, further supporting stabilization of the paratope as a means for improved NANP-repeat recognition and parasite inhibition (Figure S7E).

We conclude that core epitope recognition of the mutated antibodies is largely mediated by germline-encoded amino acids and HCDR3, whereas most affinity-matured residues do not contact the core peptide and instead stabilize the conformation of the antigen-binding site.

DISCUSSION

Humoral immunity to natural *Pf* exposure is typically short-lived and non-sterilizing, suggesting that protective B cell memory against sporozoite antigens, including CSP, is formed inefficiently. However, the potency of anti-CSP memory B cell antibodies has never been measured. Here we have shown that natural parasite exposure generated anti-CSP memory B cells that expressed *Pf* inhibitory antibodies suggesting that the overall strength of the response rather than the quality of CSP memory B cell antibodies might be insufficient to mediate long-lasting protection. The small number of parasites that were injected locally into the skin during natural *Pf* infection likely induced only weak anti-CSP immune responses that were further suppressed by the strong immune responses elicited by the high load of systemic antigen from asexual blood stage parasites (Foquet et al., 2014; Keitany et al., 2016; Scholzen and Sauerwein, 2013). Further, we have provided evidence that clonally expanded cell clusters expressing potent anti-NANP repeat antibodies could persist in the same donor over years demonstrating that the induction of high-quality and stable memory B cells is rare but possible. However, memory B cells protect from infection only indirectly upon antigen-mediated reactivation and differentiation into antibody secreting cells. This process takes several days, whereas liver cell infection is established within hours after sporozoite inoculation. Thus, the complexity of the parasite life cycle rather than the inability of the human immune system to induce memory B cells expressing protective antibodies against CSP may be associated with the lack of sterilizing immunity (Hoffman et al., 2002; Mordmüller et al., 2017; Roestenberg et al., 2009; Spring et al., 2013). Repeated booster

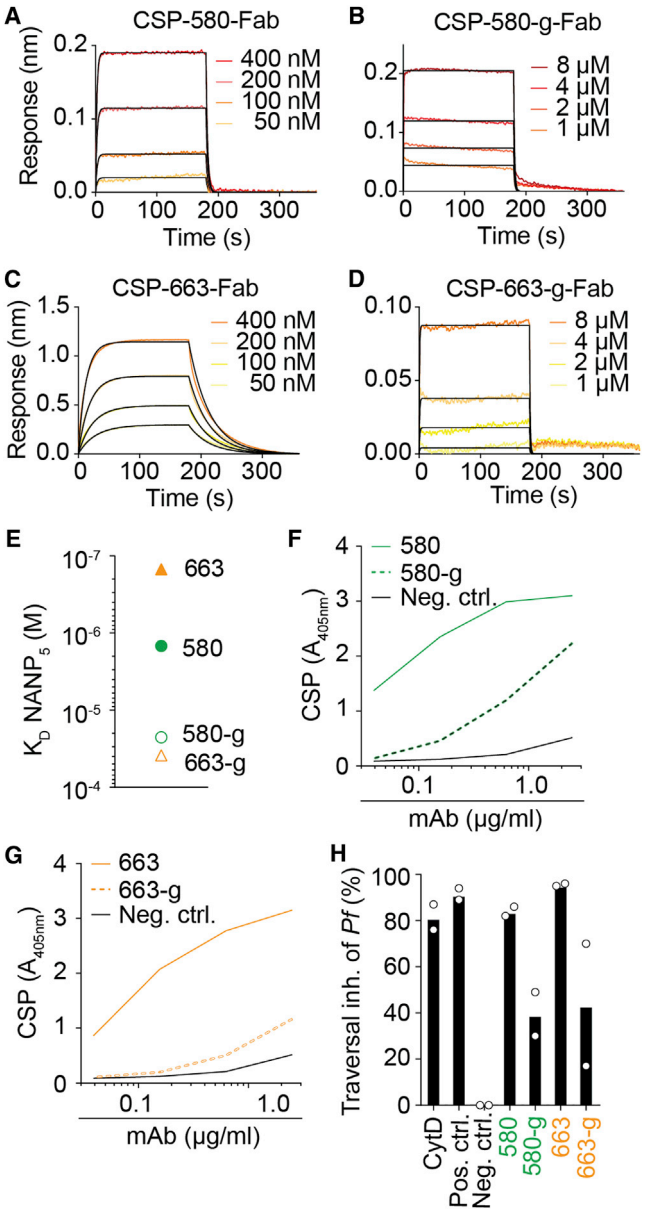

Figure 6. Functional Comparison of Affinity-Matured 580 and 663 Antibodies to Their Germline Reverted Ancestors 580-g and 663-g

(A) Representative sensograms (red and orange) and 1:1 model best fits (black) for CSP binding of the 580 Fab.

(B) Representative sensograms (red and orange) and 1:1 model best fits (black) for CSP binding of the 580-g Fab.

(C) Representative sensograms (red and orange) and 1:1 model best fits (black) for CSP binding of the 663 Fab.

(D) Representative sensograms (red and orange) and 1:1 model best fits (black) for CSP binding of the 663-g Fab.

(E) SPR against $NANP_5$ for the mutated (filled symbols) and germline (open symbols) versions of antibody 580 (circles) and 663 (triangles).

(F) CSP ELISA of the mutated (solid green line) and germline (dashed green line) versions of antibody 580.

(G) CSP ELISA of the mutated (solid orange line) and germline (dashed orange line) versions of antibody 663.

(H) *Pf* hepatocyte traversal inhibition (inh.) of the indicated antibodies. Data are from two independent experiments. Bars depict mean of two independent experiments, white circles represent mean of two technical replicates in independent experiments. Positive control antibody, Cytochalasin D (CytD) and negative control antibody are shown. Data in (A–E) and (F) and (G) are representative of two and three independent experiments, respectively. Black solid lines in (F) and (G) represent the negative control antibody. See also Table S7.

immunizations might be required to reactivate the memory B cell pool thereby indirectly sustaining sterilizing anti-CSP antibody titers that can prevent the establishment of the infection also in vaccination settings.

The antibodies identified here efficiently prevented malaria infection by inhibiting *Plasmodium* transmission from the mosquito vector to the mammalian host. During sporozoite development in the mosquito, CSP is expressed already before the invasion of salivary glands, offering an opportunity to exploit human antibodies for the development of safe and efficient vector-based transmission-blocking strategies (Sumitani et al., 2013). Because CSP is essential for sporozoite development and invasion of the salivary glands, it seems unlikely that the parasite would find mechanisms to evade antibody targeting. Further, efficient blocking of parasite infection in a series of animal models used in this study suggests that the antibodies could play an important role in mediating protection from *Pf* infection in humans. We found that antibody 580 was overall less efficacious than antibody 663 in all assays, although the differences were not significant. Future experiments will have to corroborate these findings to determine whether differences in the antigen-binding mode or affinity might correlate with efficacy. Nevertheless, our data demonstrate the power of mining the human anti-CSP antibody repertoire for better understanding of the complexity of antibody-CSP interactions and to identify molecular correlates of protection.

We found that the antibodies used primarily germline-encoded regions and the HCDR3 for recognition of the core NANP repeat suggesting that the naïve human B cell repertoire possesses the pre-requisites for effective interactions with the CSP repeat independently of excessive somatic hypermutation. Somatic hypermutations predominantly led to the stabilization of the antigen-binding site, a relatively common strategy of antibodies to improve affinity, but did not engage into direct interactions with the core epitope (Wedemayer et al., 1997). In line with these findings, repeated whole sporozoite immunizations in controlled human malaria infection of malaria naïve volunteers under chemoprophylaxis showed that protective memory B cell responses against the NANP repeat are more likely to evolve from potent germline precursors than by affinity maturation to the core epitope (Murugan et al., G.T., C.K., G.C., E. A.L., B.M., and H.W., unpublished data). Therefore, our data support vaccination strategies that seek to activate strong germline responses against the CSP repeat with immunogens designed using structure-guided approaches, similar to strategies being explored against other pathogens (Ekiert et al., 2009; Jardine et al., 2013). Taken together, our findings illustrate the power of exploring human anti-CSP antibody responses to develop tools for malaria control not only in the mammalian host but also in the mosquito vector. Future studies should assess the impact immunogens with different NANP conformations have on the quality of anti-CSP B cell responses as a basis for the development of next-generation CSP vaccines.

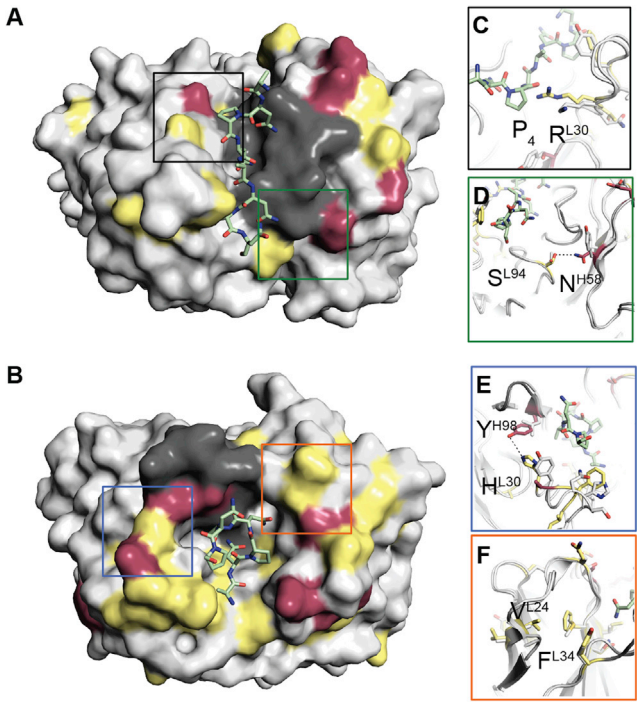

Figure 7. Structural Comparison of Affinity-Matured 580 and 663 Antibodies to Their Germline Reverted Ancestors 580-g and 663-g

(A) Surface representation of the 580-g-$NANP_5$ crystal structure. Antibody residues are colored according to identity between the germline reverted ancestors and affinity matured antibodies. Identical, similar, and different residues are colored in grey, yellow, and maroon, respectively. HCDR3 residues are colored in dark grey.

(B) Surface representation of the 663-$NANP_5$ crystal structure. Antibody residues are color-coded as in (A).

(C) Mutation in 580 that leads to additional contacts between Fab and peptide.

(D) Mutations in 580 that lead to stabilization of the paratope.

(E and F) Mutations in 663 that lead to stabilization of the paratope. See also Figure S6.

STAR★METHODS

Detailed methods are provided in the online version of this paper and include the following:

- KEY RESOURCES TABLE
- CONTACT FOR REAGENT AND RESOURCE SHARING
- EXPERIMENTAL MODEL AND SUBJECT DETAILS
  - Human Subjects
  - Cell Lines
  - Bacteria
  - *Pf* Parasites
  - Mosquito Rearing and Transgenesis
  - Mice
- METHOD DETAILS
  - Flow Cytometry and Single Cell Sorting
  - Ig Gene Cloning and Recombinant Antibodies
  - Enzyme-Linked Immunosorbent Assay
  - Generation of Chimeric *Pb* Parasites
  - Primers for the DNA Constructs for the Generation of the Chimeric Parasite Line
  - Primers for Genotyping of the Chimeric Parasite Line
  - Mosquito Transgenesis
  - *In Vivo Plasmodium* Infections
  - Immunofluorescence Assay
  - Sporozoite Hepatocyte Traversal Assay
  - Exoerythrocytic Forms Developmental Assay
  - Quantitative Real-Time (RT)-PCR
  - Immunoblotting
  - Fab Production
  - CSP Production
  - Germline Reversion
  - Biolayer Interferometry Binding Studies
  - Crystallization and Structure Determination
  - SAXS Data Collection and Processing
  - Surface Plasmon Resonance
- QUANTIFICATION AND STATISTICAL ANALYSIS
- DATA AND SOFTWARE AVAILABILITY

SUPPLEMENTAL INFORMATION

Supplemental Information includes seven figures and seven tables and can be found with this article online at https://doi.org/10.1016/j.immuni.2017.11.007.

AUTHOR CONTRIBUTION

G.T., E.A.L., J.-P.J., and H.W. designed experiments. G.T. and G.C. collected samples; G.T., S.W.S., G.C., M.P., and B.K.S. performed experiments. C.K., A.B., and R.M. provided experimental assistance. M.P. and E.M. generated transgenic *Aapp::125* mosquitoes. A.M.S., C.J.J., and S.M.K. generated *Pb-PfCSP*; S.H.I.K. provided FRG-huHep mice; B.M. and A.A.A. designed and supervised the field study; G.T., S.W.S., G.C., E.A.L., J.-P.J., and H.W. analyzed the data; G.T., S.W.S., J.-P.J., and H.W. wrote the manuscript; E.A.L., J.-P.J., and H.W. conceived the study.

ACKNOWLEDGMENTS

The authors are grateful to all study participants and thank P.G. Kremsner, B. Lell, M. Massinga Loembé, E. Askani, and members of the Albert Schweitzer Hospital and CERMEL for their support. Further, they thank Christian Busse (German Cancer Research Center, Heidelberg), Peter Sehr (EMBL-DKFZ Chemical Biology Core Facility, European Molecular Biology Laboratory, Heidelberg, Germany), Hanne Krüger, Dana Tschierske, Liane Spohr, Daniel Eyermann, and Manuela Andres (MPIIB, Berlin) for technical assistance. G.T. was supported by the International Max Planck Research School for Infectious Diseases and Immunology (IMPRS-IDI) and the German National Academic Foundation. X-ray diffraction experiments were performed using beamline 08ID-1 at the Canadian Light Source, which is supported by the Canada Foundation for Innovation, Natural Sciences and Engineering Research Council of Canada, the University of Saskatchewan, the Government of Saskatchewan, Western Economic Diversification Canada, the National Research Council Canada, and the Canadian Institutes of Health Research (CIHR). SAXS experiments were performed at beamline 18-ID of the Advanced Photon Source, a U.S. Department of Energy (DOE) Office of Science User Facility operated for the DOE Office of Science by Argonne National Laboratory under Contract No. DE-AC02-06CH11357. Part of this work was funded by NIH grant # F32 AI 114113 and by CNRS in the frame of the LIA " REL2 and resistance to malaria ". The following reagents were obtained through BEI Resources, NIAID, NIH: Hybridoma 2A10 Anti-*Plasmodium falciparum* Circumsporozoite Protein (CSP), MRA-183, contributed by Elizabeth Nardin and HC-04, Hepatocyte (human), MRA-975, contributed by Jetsumon Sattabongkot Prachumsri.

Received: May 30, 2017
Revised: August 22, 2017
Accepted: November 4, 2017
Published: November 21, 2017

SUPPORTING CITATIONS

The following references appear in the Supplemental Information: Baker et al. (2001).

REFERENCES

Adams, P.D., Afonine, P.V., Bunkóczi, G., Chen, V.B., Davis, I.W., Echols, N., Headd, J.J., Hung, L.-W., Kapral, G.J., Grosse-Kunstleve, R.W., et al. (2010). PHENIX: a comprehensive Python-based system for macromolecular structure solution. Acta Crystallogr. Sect. D Biol. Crystallogr. *66*, 213–221.

Aikawa, M., Yoshida, N., Nussenzweig, R.S., and Nussenzweig, V. (1981). The protective antigen of malarial sporozoites (Plasmodium berghei) is a differentiation antigen. J. Immunol. *126*, 2494–2495.

Aricescu, A.R., Lu, W., and Jones, E.Y. (2006). A time- and cost-efficient system for high-level protein production in mammalian cells. Acta Crystallogr. Sect. D Biol. Crystallogr. *62*, 1243–1250.

Baker, N.A., Sept, D., Joseph, S., Holst, M.J., and McCammon, J.A. (2001). Electrostatics of nanosystems: application to microtubules and the ribosome. Proc. Natl. Acad. Sci. USA *98*, 10037–10041.

Behet, M.C., Foquet, L., van Gemert, G.-J., Bijker, E.M., Meuleman, P., Leroux-Roels, G., Hermsen, C.C., Scholzen, A., and Sauerwein, R.W. (2014). Sporozoite immunization of human volunteers under chemoprophylaxis induces functional antibodies against pre-erythrocytic stages of Plasmodium falciparum. Malar. J. *13*, 136.

Bousema, T., Okell, L., Felger, I., and Drakeley, C. (2014). Asymptomatic malaria infections: detectability, transmissibility and public health relevance. Nat. Rev. Microbiol. *12*, 833–840.

Boyington, J.C., Joyce, M.G., Sastry, M., Stewart-Jones, G.B.E., Chen, M., Kong, W.-P., Ngwuta, J.O., Thomas, P.V., Tsybovsky, Y., Yang, Y., et al. (2013). Structure-Based Design of Head-Only Fusion Glycoprotein Immunogens for Respiratory Syncytial Virus. Science *342*, 592–598.

Briney, B., Sok, D., Jardine, J.G., Kulp, D.W., Skog, P., Menis, S., Jacak, R., Kalyuzhniy, O., de Val, N., Sesterhenn, F., et al. (2016). Tailored Immunogens Direct Affinity Maturation toward HIV Neutralizing Antibodies. Cell *166*, 1459–1470.e11.

Carroll, R.W., Wainwright, M.S., Kim, K.-Y., Kidambi, T., Gómez, N.D., Taylor, T., and Haldar, K. (2010). A rapid murine coma and behavior scale for quantitative assessment of murine cerebral malaria. PLoS ONE *5*, e13124.

Cerami, C., Frevert, U., Sinnis, P., Takacs, B., Clavijo, P., Santos, M.J., and Nussenzweig, V. (1992). The basolateral domain of the hepatocyte plasma membrane bears receptors for the circumsporozoite protein of Plasmodium falciparum sporozoites. Cell *70*, 1021–1033.

Cohen, J., Nussenzweig, V., Nussenzweig, R., Vekemans, J., and Leach, A. (2010). From the circumsporozoite protein to the RTS, S/AS candidate vaccine. Hum. Vaccin. *6*, 90–96.

Crompton, P.D., Moebius, J., Portugal, S., Waisberg, M., Hart, G., Garver, L.S., Miller, L.H., Barillas-Mury, C., and Pierce, S.K. (2014). Malaria immunity in man and mosquito: insights into unsolved mysteries of a deadly infectious disease. Annu. Rev. Immunol. *32*, 157–187.

de Taeye, S.W., Ozorowski, G., Torrents de la Peña, A., Guttman, M., Julien, J.P., van den Kerkhof, T.L.G.M., Burger, J.A., Pritchard, L.K., Pugach, P., Yasmeen, A., et al. (2015). Immunogenicity of Stabilized HIV-1 Envelope Trimers with Reduced Exposure of Non-neutralizing Epitopes. Cell *163*, 1702–1715.

Doolan, D.L., Dobaño, C., and Baird, J.K. (2009). Acquired immunity to malaria. Clin. Microbiol. Rev. *22*, 13–36.

Dups, J.N., Pepper, M., and Cockburn, I.A. (2014). Antibody and B cell responses to Plasmodium sporozoites. Front. Microbiol. *5*, 625.

Dyson, H.J., Satterthwait, A.C., Lerner, R.A., and Wright, P.E. (1990). Conformational preferences of synthetic peptides derived from the immunodominant site of the circumsporozoite protein of Plasmodium falciparum by 1H NMR. Biochemistry *29*, 7828–7837.

Ekiert, D.C., Bhabha, G., Elsliger, M.-A., Friesen, R.H.E., Jongeneelen, M., Throsby, M., Goudsmit, J., and Wilson, I.A. (2009). Antibody recognition of a highly conserved influenza virus epitope. Science *324*, 246–251.

Emsley, P., Lohkamp, B., Scott, W.G., and Cowtan, K. (2010). Features and development of Coot. Acta Crystallogr. D Biol. Crystallogr. *66*, 486–501.

Escolano, A., Steichen, J.M., Dosenovic, P., Kulp, D.W., Golijanin, J., Sok, D., Freund, N.T., Gitlin, A.D., Oliveira, T., Araki, T., et al. (2016). Sequential Immunization Elicits Broadly Neutralizing Anti-HIV-1 Antibodies in Ig Knockin Mice. Cell *166*, 1445–1458.e12.

Fisher, C.R., Sutton, H.J., Kaczmarski, J.A., McNamara, H.A., Clifton, B., Mitchell, J., Cai, Y., Dups, J.N., D'Arcy, N.J., Singh, M., et al. (2017). T-dependent B cell responses to Plasmodium induce antibodies that form a high-avidity multivalent complex with the circumsporozoite protein. PLoS Pathog. *13*, e1006469.

Foquet, L., Hermsen, C.C., van Gemert, G.J., Van Braeckel, E., Weening, K.E., Sauerwein, R., Meuleman, P., and Leroux-Roels, G. (2014). Vaccine-induced monoclonal antibodies targeting circumsporozoite protein prevent Plasmodium falciparum infection. J. Clin. Invest. *124*, 140–144.

Fraiture, M., Baxter, R.H.G., Steinert, S., Chelliah, Y., Frolet, C., Quispe-Tintaya, W., Hoffmann, J.A., Blandin, S.A., and Levashina, E.A. (2009). Two mosquito LRR proteins function as complement control factors in the TEP1-mediated killing of Plasmodium. Cell Host Microbe *5*, 273–284.

Frank, K., and Sippl, M.J. (2008). High-performance signal peptide prediction based on sequence alignment techniques. Bioinformatics *24*, 2172–2176.

Franke, D., and Svergun, D.I. (2009). DAMMIF, a program for rapid ab-initio shape determination in small-angle scattering. J. Appl. Cryst. *42*, 342–346.

Frevert, U., Sinnis, P., Cerami, C., Shreffler, W., Takacs, B., and Nussenzweig, V. (1993). Malaria circumsporozoite protein binds to heparan sulfate proteoglycans associated with the surface membrane of hepatocytes. J. Exp. Med. *177*, 1287–1298.

Ghasparian, A., Moehle, K., Linden, A., and Robinson, J.A. (2006). Crystal structure of an NPNA-repeat motif from the circumsporozoite protein of the malaria parasite Plasmodium falciparum. Chem. Commun. (Camb.) *3*, 174–176.

Harris, C., Lambrechts, L., Rousset, F., Abate, L., Nsango, S.E., Fontenille, D., Morlais, I., and Cohuet, A. (2010). Polymorphisms in Anopheles gambiae immune genes associated with natural resistance to Plasmodium falciparum. PLoS Pathog. *6*, e1001112.

Hoffman, S.L., Goh, L.M.L., Luke, T.C., Schneider, I., Le, T.P., Doolan, D.L., Sacci, J., de la Vega, P., Dowler, M., Paul, C., et al. (2002). Protection of humans against malaria by immunization with radiation-attenuated Plasmodium falciparum sporozoites. J. Infect. Dis. *185*, 1155–1164.

Ikpa, T.F., and Adebambo, A.A. (2011). Immunoglobulin G subclass responses to Plasmodium falciparum circumsporozoite protein among Nigerian children. Int. J. Trop. Med. *6*, 100–105.

Ishizuka, A.S., Lyke, K.E., DeZure, A., Berry, A.A., Richie, T.L., Mendoza, F.H., Enama, M.E., Gordon, I.J., Chang, L.-J., Sarwar, U.N., et al. (2016). Protection against malaria at 1 year and immune correlates following PfSPZ vaccination. Nat. Med. *22*, 614–623.

Janse, C.J., Ramesar, J., and Waters, A.P. (2006). High-efficiency transfection and drug selection of genetically transformed blood stages of the rodent malaria parasite Plasmodium berghei. Nat. Protoc. *1*, 346–356.

Jardine, J., Julien, J.P., Menis, S., Ota, T., Kalyuzhniy, O., McGuire, A., Sok, D., Huang, P.S., MacPherson, S., Jones, M., et al. (2013). Rational HIV immunogen design to target specific germline B cell receptors. Science *340*, 711–716.

John, C.C., Tande, A.J., Moormann, A.M., Sumba, P.O., Lanar, D.E., Min, X.M., and Kazura, J.W. (2008). Antibodies to pre-erythrocytic Plasmodium falciparum antigens and risk of clinical malaria in Kenyan children. J. Infect. Dis. *197*, 519–526.

Kabsch, W. (2010). XDS. Acta Crystallogr. D Biol. Crystallogr. *66*, 125–132.

Keitany, G.J., Kim, K.S., Krishnamurty, A.T., Hondowicz, B.D., Hahn, W.O., Dambrauskas, N., Sather, D.N., Vaughan, A.M., Kappe, S.H.I., and Pepper,

M. (2016). Blood Stage Malaria Disrupts Humoral Immunity to the Pre-erythrocytic Stage Circumsporozoite Protein. Cell Rep. *17*, 3193–3205.

Konarev, P.V., Volkov, V.V., Sokolova, A.V., Koch, M.H.J., and Svergun, D.I. (2003). PRIMUS: a Windows PC-based system for small-angle scattering data analysis. J. Appl. Cryst. *36*, 1277–1282.

Krishnamurty, A.T., Thouvenel, C.D., Portugal, S., Keitany, G.J., Kim, K.S., Holder, A., Crompton, P.D., Rawlings, D.J., and Pepper, M. (2016). Somatically Hypermutated Plasmodium-Specific IgM(+) Memory B Cells Are Rapid, Plastic, Early Responders upon Malaria Rechallenge. Immunity *45*, 402–414.

Lackner, P., Beer, R., Heussler, V., Goebel, G., Rudzki, D., Helbok, R., Tannich, E., and Schmutzhard, E. (2006). Behavioural and histopathological alterations in mice with cerebral malaria. Neuropathol. Appl. Neurobiol. *32*, 177–188.

Langhorne, J., Ndungu, F.M., Sponaas, A.-M., and Marsh, K. (2008). Immunity to malaria: more questions than answers. Nat. Immunol. *9*, 725–732.

Lin, J.W., Annoura, T., Sajid, M., Chevalley-Maurel, S., Ramesar, J., Klop, O., Franke-Fayard, B.M.D., Janse, C.J., Khan, S.M., Carvalho, T., et al. (2011). A novel 'gene insertion/marker out' (GIMO) method for transgene expression and gene complementation in rodent malaria parasites. PLoS ONE *6*, e29289.

McCoy, A.J., Grosse-Kunstleve, R.W., Adams, P.D., Winn, M.D., Storoni, L.C., and Read, R.J. (2007). Phaser crystallographic software. J. Appl. Cryst. *40*, 658–674.

Ménard, R., Sultan, A.A., Cortes, C., Altszuler, R., van Dijk, M.R., Janse, C.J., Waters, A.P., Nussenzweig, R.S., and Nussenzweig, V. (1997). Circumsporozoite protein is required for development of malaria sporozoites in mosquitoes. Nature *385*, 336–340.

Mordmüller, B., Surat, G., Lagler, H., Chakravarty, S., Ishizuka, A.S., Lalremruata, A., Gmeiner, M., Campo, J.J., Esen, M., Ruben, A.J., et al. (2017). Sterile protection against human malaria by chemoattenuated PfSPZ vaccine. Nature *542*, 445–449.

Morin, A., Eisenbraun, B., Key, J., Sanschagrin, P.C., Timony, M.A., Ottaviano, M., and Sliz, P. (2013). Collaboration gets the most out of software. eLife *2*, e01456.

Muellenbeck, M.F., Ueberheide, B., Amulic, B., Epp, A., Fenyo, D., Busse, C.E., Esen, M., Theisen, M., Mordmüller, B., and Wardemann, H. (2013). Atypical and classical memory B cells produce Plasmodium falciparum neutralizing antibodies. J. Exp. Med. *210*, 389–399.

Nielsen, H. (2017). Predicting Secretory Proteins with SignalP. In Methods Mol Biol (New York, NY: Humana Press), pp. 59–73.

Noland, G.S., Jansen, P., Vulule, J.M., Park, G.S., Ondigo, B.N., Kazura, J.W., Moormann, A.M., and John, C.C. (2015). Effect of transmission intensity and age on subclass antibody responses to Plasmodium falciparum pre-erythrocytic and blood-stage antigens. Acta Trop. *142*, 47–56.

Offeddu, V., Thathy, V., Marsh, K., and Matuschewski, K. (2012). Naturally acquired immune responses against Plasmodium falciparum sporozoites and liver infection. Int. J. Parasitol. *42*, 535–548.

Planche, T., Krishna, S., Kombila, M., Engel, K., Faucher, J.F., Ngou-Milama, E., Kremsner, P.G., Hospital, A.S., and Humanparasitologie, S. (2001). Comparison of methods for the rapid laboratory assessment of children with malaria. Am. J. Trop. Med. Hyg. *65*, 599–602.

Pompon, J., and Levashina, E.A. (2015). A New Role of the Mosquito Complement-like Cascade in Male Fertility in Anopheles gambiae. PLoS Biol. *13*, e1002255.

Portugal, S., Pierce, S.K., and Crompton, P.D. (2013). Young lives lost as B cells falter: what we are learning about antibody responses in malaria. J. Immunol. *190*, 3039–3046.

Roestenberg, M., McCall, M., Hopman, J., Wiersma, J., Luty, A.J.F., van Gemert, G.J., van de Vegte-Bolmer, M., van Schaijk, B., Teelen, K., Arens, T., et al. (2009). Protection against a malaria challenge by sporozoite inoculation. N. Engl. J. Med. *361*, 468–477.

RTS,S Clinical Trials Partnership (2015). Efficacy and safety of RTS,S/AS01 malaria vaccine with or without a booster dose in infants and children in Africa: final results of a phase 3, individually randomised, controlled trial. Lancet *386*, 31–45.

Sack, B.K., Mikolajczak, S.A., Fishbaugher, M., Vaughan, A.M., Flannery, E.L., Nguyen, T., Betz, W., Navarro, M.J., Foquet, L., Steel, R.W.J., Billman, Z.P., Murphy, S.C., Hoffman, S.L., Chakravarty, S., Sim, B.K.L., Behet, M., Reuling, I.J., Walk, J., Scholzen, A., Sauerwein, R.W., Ishizuka, A.S., Flynn, B., Seder, R.A., and Kappe, S.H.I. (2017). Humoral protection against mosquito bite-transmitted Plasmodium falciparum infection in humanized mice. npj Vaccines *27*, https://doi.org/10.1038/s41541-017-0028-2.

Salman, A.M., Mogollon, C.M., Lin, J., van Pul, F.J.A., Janse, C.J., and Khan, S.M. (2015). Generation of Transgenic Rodent Malaria Parasites Expressing Human Malaria Parasite Proteins. In Malaria Vaccines. Methods in Molecular Biology, *Volume 1325*, A. Vaughan, ed. (New York, NY, USA: Humana Press), pp. 257–286.

Sattabongkot, J., Yimamnuaychoke, N., Leelaudomlipi, S., Rasameesoraj, M., Jenwithisuk, R., Coleman, R.E., Udomsangpetch, R., Cui, L., and Brewer, T.G. (2006). Establishment of a human hepatocyte line that supports in vitro development of the exo-erythrocytic stages of the malaria parasites Plasmodium falciparum and P. vivax. Am. J. Trop. Med. Hyg. *74*, 708–715.

Scholzen, A., and Sauerwein, R.W. (2013). How malaria modulates memory: activation and dysregulation of B cells in Plasmodium infection. Trends Parasitol. *29*, 252–262.

Sidjanski, S.P., Vanderberg, J.P., and Sinnis, P. (1997). Anopheles stephensi salivary glands bear receptors for region I of the circumsporozoite protein of Plasmodium falciparum. Mol. Biochem. Parasitol. *90*, 33–41.

Spring, M., Murphy, J., Nielsen, R., Dowler, M., Bennett, J.W., Zarling, S., Williams, J., de la Vega, P., Ware, L., Komisar, J., et al. (2013). First-in-human evaluation of genetically attenuated Plasmodium falciparum sporozoites administered by bite of Anopheles mosquitoes to adult volunteers. Vaccine *31*, 4975–4983.

Struik, S.S., and Riley, E.M. (2004). Does malaria suffer from lack of memory? Immunol. Rev. *201*, 268–290.

Sumitani, M., Kasashima, K., Yamamoto, D.S., Yagi, K., Yuda, M., Matsuoka, H., and Yoshida, S. (2013). Reduction of malaria transmission by transgenic mosquitoes expressing an antisporozoite antibody in their salivary glands. Insect Mol. Biol. *22*, 41–51.

Tewari, K., Flynn, B.J., Boscardin, S.B., Kastenmueller, K., Salazar, A.M., Anderson, C.A., Soundarapandian, V., Ahumada, A., Keler, T., Hoffman, S.L., et al. (2010). Poly(I:C) is an effective adjuvant for antibody and multi-functional CD4+ T cell responses to Plasmodium falciparum circumsporozoite protein (CSP) and αDEC-CSP in non human primates. Vaccine *28*, 7256–7266.

Tian, M., Cheng, C., Chen, X., Duan, H., Cheng, H.L., Dao, M., Sheng, Z., Kimble, M., Wang, L., Lin, S., et al. (2016). Induction of HIV Neutralizing Antibody Lineages in Mice with Diverse Precursor Repertoires. Cell *166*, 1471–1484.e18.

Tiller, T., Meffre, E., Yurasov, S., Tsuiji, M., Nussenzweig, M.C., and Wardemann, H. (2008). Efficient generation of monoclonal antibodies from single human B cells by single cell RT-PCR and expression vector cloning. J. Immunol. Methods *329*, 112–124.

Vaughan, A.M., Mikolajczak, S.A., Wilson, E.M., Grompe, M., Kaushansky, A., Camargo, N., Bial, J., Ploss, A., and Kappe, S.H.I. (2012a). Complete Plasmodium falciparum liver-stage development in liver-chimeric mice. J. Clin. Invest. *122*, 3618–3628.

Vaughan, A.M., Mikolajczak, S.A., Camargo, N., Lakshmanan, V., Kennedy, M., Lindner, S.E., Miller, J.L., Hume, J.C., and Kappe, S.H. (2012b). A transgenic Plasmodium falciparum NF54 strain that expresses GFP-luciferase throughout the parasite life cycle. Mol. Biochem. Parasitol. *186*, 143–147.

Volkov, V.V., and Svergun, D.I. (2003). Uniqueness of ab-initio shape determination in small-angle scattering. J. Appl. Cryst. *36*, 860–864.

Volohonsky, G., Terenzi, O., Soichot, J., Naujoks, D. a, Nolan, T., Windbichler, N., Kapps, D., Smidler, A.L., Vittu, A., Costa, G., et al. (2015). Tools for Anopheles gambiae Transgenesis. G3 (Bethesda) *5*, 1151–1163.

Wardemann, H., Yurasov, S., Schaefer, A., Young, J.W., Meffre, E., and Nussenzweig, M.C. (2003). Predominant autoantibody production by early human B cell precursors. Science *301*, 1374–1377.

Wedemayer, G.J., Patten, P.A., Wang, L.H., Schultz, P.G., and Stevens, R.C. (1997). Structural Insights into the Evolution of an Antibody Combining Site. Science *276*, 1665–1669.

White, M.T., Bejon, P., Olotu, A., Griffin, J.T., Riley, E.M., Kester, K.E., Ockenhouse, C.F., and Ghani, A.C. (2013). The relationship between RTS,S vaccine-induced antibodies, $CD4^+$ T cell responses and protection against Plasmodium falciparum infection. PLoS ONE *8*, e61395.

Ye, J., Ma, N., Madden, T.L., and Ostell, J.M. (2013). IgBLAST: an immunoglobulin variable domain sequence analysis tool. Nucleic Acids Res. *41*, W34–W40.

Yoshida, S., and Watanabe, H. (2006). Robust salivary gland-specific transgene expression in Anopheles stephensi mosquito. Insect Mol. Biol. *15*, 403–410.

Yoshida, N., Nussenzweig, R.S., Potocnjak, P., Nussenzweig, V., and Aikawa, M. (1980). Hybridoma produces protective antibodies directed against the sporozoite stage of malaria parasite. Science *207*, 71–73.

Zavala, F., Cochrane, A.H., Nardin, E.H., Nussenzweig, R.S., and Nussenzweig, V. (1983). Circumsporozoite proteins of malaria parasites contain a single immunodominant region with two or more identical epitopes. J. Exp. Med. *157*, 1947–1957.

STAR★METHODS

KEY RESOURCES TABLE

REAGENT or RESOURCE	SOURCE	IDENTIFIER
Antibodies		
Goat anti-human IgG, Fcγ	Jackson ImmunoResearch	Cat# 109-005-098; RRID: AB_2337541
Goat anti-human IgG, Fcγ (HRP conjugated)	Jackson ImmunoResearch	Cat# 109-035-098; RRID: AB_2337586
Goat anti-human IgM, Fc5μ (HRP conjugated)	Jackson ImmunoResearch	Cat# 109-035-043
Mouse anti-human CD19 (PE-Cy7 conjugated) (SJ25C1)	Thermo Fischer Scientific	Cat# 25-0198-41; RRID: AB_10671548
Mouse anti-human CD21 (PE-conjugated) (HB5)	Thermo Fischer Scientific	Cat# 12-0219-41; RRID: AB_1548734
Mouse anti-human CD27 (FITC-conjugated) (Clone: M-T271)	BD Biosciences	Cat# 560986; RRID: AB_10562556
Mouse anti-human IgG (Biotin conjugated) (Clone: G18-145)	BD Biosciences	Cat# 555785; RRID: AB_396120
Qdot®605-Streptavidin	Thermo Fischer Scientific	Cat# Q10101MP
Alexa555® conjugated goat anti-mouse IgG	Thermo Fischer Scientific	Cat#A-21422; RRID: RRID: AB_141822
AlexaFluor488® conjugated goat anti-mouse IgG	Thermo Fischer Scientific	Cat# A-11001; RRID: AB_2534069
Cy3-conjugated goat anti-human IgG (H+L)	Jackson ImmunoResearch	Cat# 109-165-003; RRID: AB_2337718
Rabbit anti-GFP	Abcam	Cat# ab290; RRID: AB_303395
Human recombinant mG053	Wardemann et al., 2003	N/A
Mouse anti-Pb CSP (clone 3D11)	BEI Resources	MRA-100, contributed by Victor Nussenzweig
Mouse anti-Pf CSP (clone 2A10)	BEI Resources	MRA-183, contributed by Elizabeth Nardin
Humanized recombinant anti-Pf CSP (clone 2A10)	Zavala et al., 1983, Self-made	N/A
Rabbit anti-*A. gambiae* Prophenoloxidase 2	Fraiture et al., 2009	N/A
Goat anti-Rabbit IgG (H+L) Poly-HRP	Pierce	Cat# 32260; RRID: AB_1965959
Rabbit anti-Flag	Sigma Aldrich	Cat# F7425; RRID: AB_439687
Bacterial and Virus Strains		
MAX Efficiency® DH10B™ Competent Cells	Thermo Fischer Scientific	Cat# 18297010
Biological Samples		
Human Peripheral blood mononucleocytes	Collected for this study and obtained from the trial Bmem2010 (Muellenbeck et al., 2013)	N/A
Chemicals, Peptides, and Recombinant Proteins		
7AAD	Thermo Fischer Scientific	Cat# A1310
ABTS tablets	Roche	Cat# 11112422001
7G8 *Pf* CSP	This paper, p. 45	N/A
NF54 *Pf* CSP	kind gift of B. Kim Lee Sim	N/A
(NANP)10	Alpha Diagnostic International	Cat# NANP101-P
(NANP)5	Alpha Diagnostic International	Cat# NANP51-P
(NANP)5	Genscript	N/A
Pf dNCSP	Tewari et al., 2010	N/A
MSP3	kind gift of Michael Theissen	N/A
Dextran, Tetramethylrhodamine, 10,000 MW, Lysine Fixable (fluoro-Ruby)	Thermo Fischer Scientific	Cat# D-1817
Cytochalasin D	Sigma Aldrich	Cat# C8273
Amphotericin B (Fungizone)	Gibco	Cat# 15290-018
DAPI	Molecular Probes	Cat# D1306; RRID: AB_2629482

(*Continued on next page*)

Continued

REAGENT or RESOURCE	SOURCE	IDENTIFIER
Sensor Chip CM5	GE Healthcare	Cat# BR100530
Insulin	Sigma Aldrich	Cat# I9278-5ML
LPS	Sigma Aldrich	Cat# L2637-5MG
FectoPRO®	Polyplus	Cat# 116-040
Critical Commercial Assays		
Protein G Sepharose 4 Fast Flow	GE Healthcare	Cat# 17-0618-06
Protein A affinity chromatography	GE Healthcare	Cat# 17-5280-01
HisTrap FF	GE Healthcare	Cat# 17-5255-01
Superdex 200 Increase 10/300 GL	GE Healthcare	Cat# 28990944
HiTrap Protein A HP	GE Healthcare	Cat# 17-0402-01
MonoS 10/100 GL	GE Healthcare	Cat# 17-5169-01
Alexa Fluor® 647 Protein Labeling Kit	Thermo Fischer Scientific	Cat# A20173
NucleoSpin® 96 PCR Clean-Up	Macherey-Nagel	Cat# 740658.24
NucleoSpin® Gel and PCR Clean-up	Macherey-Nagel	Cat# 740609.50
NucleoSpin® Plasmid Kit	Macherey-Nagel	Cat# 740588.250
PureLink™ HiPure Plasmid Maxiprep Kit	Invitrogen	Cat# 2018-06-30
Human Antibody Capture Kit	GE Healthcare	Cat# BR100839
Ni-NTA (NTA) Dip and Read™ Biosensors	FortéBio	Cat# 18-5101
RevertAid H Minus Reverse Transcriptase kit	Thermo Fischer Scientific	Cat# EP0451
Deposited Data		
Crystal structures	Protein Data Bank	PDB codes: 6AZM, 5BK0, 5BK3, 5BK5, 6AZX
Experimental Models: Cell Lines		
2A10 Hybridoma	BEI Resources	MRA-183, contributed by Elizabeth Nardin
HEK-293F	Thermo Fischer Scientific	Cat# R79007
HEK-293T	DSMZ	Cat# ACC-635; RRID: CVCL_0063
HC-04	BEI Resources	MRA-975, contributed by Jetsumon Sattabongkot Prachumsri
Experimental Models: Organisms/Strains		
Pf NF54	a kind gift of Dr. R. Sauerwein	N/A
Pf GFP-luc	Vaughan et al., 2012b	N/A
Pb GFP-luc	Janse et al., 2006	RMgm 29
Pb-PfCSP	This paper, p. 36-39	PbANKA-PfCSP(r)PbCSP (2257cl2); RMgm 4110
A. coluzzii (Ngousso strain) mosquitoes	Harris et al., 2010	N/A
A. stephensi mosquitoes		
A. gambiae 7b mosquitoes	Pompon and Levashina, 2015	N/A
A. coluzzii Aapp::125 mosquitoes	This paper, p. 39-40	N/A
FRG-huHep mice	Yecuris, Inc.	N/A
Female C57BL/6J mice	Charles River Laboratories	Cat# 000664; RRID:IMSR_JAX:000664
Oligonucleotides		
Primers for Ig genes nested PCR, cloning and sequencing	Tiller et al., 2008	N/A
Primers for the generation of a humanized version of the antibody 2A10	This paper, p. 35-36	N/A
Primers for generation and phenotyping of chimeric *Pb* parasites	This paper, p. 37-39	N/A
Primers for Quantitative Real-Time PCR in *A. coluzzii*	This paper, p. 43	N/A

(*Continued on next page*)

Continued

REAGENT or RESOURCE	SOURCE	IDENTIFIER
Recombinant DNA		
IGγ1-, IGκ- or IGλ-expression vectors	Tiller et al., 2008	N/A
pHLsec	Aricescu et al., 2006	N/A
Software and Algorithms		
Prism 6.07	GraphPad	http://www.graphpad.com
R version 0.99.484	The R project for statistical computing	http://www.R-project.org/
FACSDiVa version 8.0.1	Becton Dickinson	Cat# 659528
FlowJo version V.10.0.8	Tree Star	https://www.flowjo.com/solutions/flowjo/downloads
ImageJ	Rasband, 1997-2015	https://imagej.nih.gov/ij/download.html
Adobe Illustrator CS6 v16.0.3	Adobe	http://www.adobe.com/de/products/illustrator.html
LivingImaging	N/A	www.perkinelmer.de
AxioVision ZEN 2012 software	Zeiss	https://www.zeiss.com/microscopy/int/products/microscope-software/zen-lite.html
IgBlast	Ye et al., 2013	https://www.ncbi.nlm.nih.gov/igblast/
Octet Data Analysis Software 9.0.0.6	FortéBio	https://www.fortebio.com/octet-software.html
XDS	Kabsch, 2010	http://xds.mpimf-heidelberg.mpg.de
Phaser	McCoy et al., 2007	https://www.phenix-online.org
Phenix	Adams et al., 2010	https://www.phenix-online.org
Coot	Emsley et al., 2010	https://www2.mrc-lmb.cam.ac.uk/personal/pemsley/coot/
SBGrid	Morin et al., 2013	https://sbgrid.org
Pymol	The PyMOL Molecular Graphics System, Version 1.8 Schrödinger, LLC.	https://pymolwiki.org/index.php/Main_Page
PRIMUS	Konarev et al., 2003	https://www.embl-hamburg.de/biosaxs/primus.html
DAMMIF	Franke and Svergun, 2009	https://www.embl-hamburg.de/biosaxs/dammif.html
DAMAVER	Volkov and Svergun, 2003	https://www.embl-hamburg.de/biosaxs/damaver.html
SignalP 4.1 Server	Nielsen, 2017	http://www.cbs.dtu.dk/services/SignalP/
Signal Blast programs	Frank and Sippl , 2008	http://sigpep.services.came.sbg.ac.at/signalblast.html
GENEius	Biolink Informationstechnologie GmbH (Eurofins)	https://www.eurofinsgenomics.eu/en/gene-synthesis-molecular-biology/geneius.aspx

CONTACT FOR REAGENT AND RESOURCE SHARING

Further information and requests for resources and reagents should be directed to and will be fulfilled by the Lead Contact, Hedda Wardemann (h.wardemann@dkfz.de).

EXPERIMENTAL MODEL AND SUBJECT DETAILS

Human Subjects

Healthy adult male and female volunteers (mean age 33.5 +/-15 (SD) years ranging from 18 to 85 years) were recruited during the dry season (June-July 2014) in the greater area of Lambaréné, Gabon, Africa. Ethical approval was obtained by the Comité d'Ethique Régional Indépendant de Lambaréné (No.006/2014) and the study was conducted according to the principles of the Declaration

of Helsinki. Volunteers who provided written informed consent following information about the study were screened. Inclusion criteria were: age >18 years, hemoglobin concentration >10g/dl, negative thick blood smear (Planche et al., 2001) and no acute symptoms of disease. Exclusion criteria were: pregnancy, chronic infection, autoimmune disease, previous participation in a malaria vaccine trial, cancer and immunosuppressive therapy. In addition, samples collected in July-August 2010 during the Bmem2010 study were used (Muellenbeck et al., 2013). Some of the study participants of the Bmem2010 study, including donor 71, were re-sampled during the dry-season of 2012.

Cell Lines

Human embryonic kidney HEK 293 T cells were cultured according to the manufacturer's instructions. The cells were grown at 37 °C and 8% CO_2. The hepatocyte cell line HC04 (Sattabongkot et al., 2006) was cultured at 37 °C and 5% CO_2 using HC04 complete culture medium. This comprises of 428.75 ml MEM (- L-glu), 428.75 ml F-12 Nutrient Mix (+ L-glu), 15 mM HEPES, 1.5 g/l NaHCO3, 2.5 mM L-glutamine and 10% FCS. See "Key Resources Table" for details. Cell lines have not been authenticated.

Bacteria

MAX Efficiency® DH10B™ Competent Cells were grown in LB medium for cultivation and in Terrific Broth for plasmid purification. Bacterial shaker at 37 °C and 180 rpm was used for cultivation.

Pf Parasites

Pf NF54 (a kind gift of Dr. R. Sauerwein) and *PfGFP-luc* (Vaughan et al., 2012b) were used throughout this study. For gametocyte production, asynchronous parasites were diluted to 0.8-1% parasitaemia and cultured for 15-17 days before mosquito infections.

Mosquito Rearing and Transgenesis

All mosquitoes were kept at 27-29 °C and 70-80% humidity. *A. coluzzii* (Ngousso strain) mosquitoes were used for the production of *Pf* NF54 sporozoites for traversal and IFA assays. *A. coluzzii* (Ngousso strain) XK docking line was used for transgenesis (Volohonsky et al., 2015). *A. stephensi* mosquitoes were used for experiments with humanized FRG-huHep mice (see also Figure 3E) and for the phenotypic analysis of *Pb-PfCSP* parasites (see also Figures S6E and S6H). *A. gambiae* 7b mosquitoes (Pompon and Levashina, 2015), an immunocompromised transgenic mosquito line derived from the G3 laboratory strain, were used for the characterization and production of *Pb-PfCSP* sporozoites.

Mice

Female C57BL/6J mice (8-weeks old) were purchased from Charles River and handled in accordance with the German Animal Protection Law (§8 Tierschutzgesetz) and approved by the Landesamt für Gesundheit und Soziales (Lageso), Berlin, Germany (project numbers 411/08 and 0027/12). FRG-huHep mice were purchased from Yecuris, Inc. with a minimum serum human albumin concentration of 3 mg/ml, indicating robust human hepatocyte repopulation. See "Key Resources Table" for details. Littermates were randomly assigned to experimental groups which were kept in separate cages.

METHOD DETAILS

Flow Cytometry and Single Cell Sorting

Peripheral blood was obtained by venous puncture from participants positive for anti-CSP serum antibodies. For donor 71 we obtained and used a second blood sample that was collected two years later. Peripheral mononuclear cells (PBMCs) were isolated using Percoll gradient density centrifugation (GE Healthcare). NF54 *Pf* CSP (Protein Potential LLC) and MSP3 were chemically coupled to Alexa647 according to the manufacturer's protocol (Invitrogen). Protein concentrations were determined using Nanodrop (Thermo Scientific). CSP-reactive or MSP3-reactive memory B cells were analyzed on a LSR II instrument and isolated using an ARIA II cell sorter (BD Bioscience). Cells were stained using CSP-Alex647 (1:20; 0.6mg/ml) or MSP3-Alexa647 (1:20; 0.3mg/ml) and the following antibodies: mouse anti-human CD19-PeCy7 (1:20, eBioscience), mouse anti-human CD27-FITC (1:5, BD) and mouse anti-human IgG-Biotin (1:200, BD). Biotin was detected using Streptavidin $Qdot_{605}$ (1:800, Life Technologies). 7AAD (1:200, Invitrogen) was included in all stainings to exclude dead cells. The data were analyzed using FlowJo v10 software. For single-cell sorting, CSP-reactive memory B cells were defined as $7AAD^-CSP^+CD19^+CD27^+IgG^+$, $7AAD^-CSP^+CD19^+CD27^+$ IgG^- and $7AAD^-CSP^+CD19^+CD27^-IgG^+$. $7AAD^-CSP^+CD19^+CD27^+$ IgG^- cells were later confirmed to be IgM^+ by sequence analysis. As all three cell populations were isolated based on CSP-reactivity and thus Ig surface expression, we define them as CSP-reactive memory B cells.

Ig Gene Cloning and Recombinant Antibodies

Ig gene cloning and recombinant antibody production were performed as described before (Tiller et al., 2008). In brief, cDNA of each single cell was generated using random hexamer primers. Ig heavy and corresponding Ig kappa or Ig lambda L-chain gene transcripts were amplified using a semi-nested PCR strategy (Tiller et al., 2008). Amplicons were Sanger sequenced and cloned into human $Ig\gamma1$ and $Ig\kappa$ or $Ig\lambda$ expression vectors, respectively (Tiller et al., 2008). The corresponding heavy and light expression vector DNAs were co-transfected into HEK293T cells (Invitrogen) and the recombinant antibodies were purified from supernatants using Protein G beads (GE Healthcare). IgG concentrations were determined by ELISA.

To generate a humanized version of the antibody 2A10 to use as a positive control cells from a murine 2A10 hybridoma cell line (BEI Resources) were harvested and RNA was extracted according to the manufacturer's protocol (Macherey Nagel). cDNA was generated as described previously (Tiller et al., 2008). Ig gene transcripts of the H- and kappa L-chain were amplified using the following primers: heavy forward primer mIghV-Y/AgeI-081-fw: 5'-*CTGCAACCGGTGTACATTCCCAGATCCAGTTGGTACAGTCTGG*-3', reverse primer mIghJ-D/SalI-034-rv: 5'-*TGCGAAGTCGACGCTGAGGAGACGGTGACTGAGG*-3', kappa forward primer mIgkV-P/AgeI-084-fw: 5'-*CTGCAACCGGTGTACATTCCGATATCCAGATGACACAGA CTACA*-3' and kappa revers primer: mIgkJ-B/BsiWI-020-rv: 5'-*GCCACCGTACGTTTTATTTCC AGCTTGGTC*-3'. Gene transcripts were sequenced and cloned into the human Igγ1 and Igκ expression vectors. Antibody was then expressed and purified as described above.

Enzyme-Linked Immunosorbent Assay

96 well plates (Costar) were coated overnight at 4 °C with 40 ng/well of N-terminally truncated *Pf* CSP (CSP) with the amino acids 123-411 (kind gift from Silvia Boscardin) (Tewari et al., 2010), 100 ng/well $NANP_{10}$-repeat (Alpha Diagnostic Intl Inc.), 10 μg/ml insulin (Sigma Aldrich) or 5 μg/ml LPS (Sigma Aldrich) solution in PBS. ELISA plates were blocked for 1 h with 4% BSA in PBS (serum ELISA), 1% BSA in PBS (antigen ELISA) or blocking buffer (1x PBS, 0.05% (v/v) Tween20, 1 mM EDTA) (IgG concentration ELISA). Coated plates were incubated with the serum or recombinant monoclonal antibodies at the indicated concentrations for 1 h at RT. Bound antibodies were detected by goat anti-human IgG or goat anti-human IgM secondary antibody coupled to horse-radish-peroxidase (HRP) (Jackson Immuno Research) diluted 1:1,000 in 1% BSA in PBS which was then detected using an ABTS substrate solution complimented with H_2O_2 (Roche). The optical density (OD) at 405 nm was determined on an M1000Pro plate reader (Tecan). Graphs were created and area under curve (AUC) values were calculated using GraphPad Prism 6.07. 2A10 (Zavala et al., 1983) was used as a positive and mGO53 (Wardemann et al., 2003) as a negative control.

Generation of Chimeric *Pb* Parasites

To generate the chimeric parasites where the *Pb csp* coding sequence (CDS) (*Pbcsp*; PBANKA_0403200) has been replaced by the *Pf csp* CDS (*Pfcsp*; PF3D7_0304600), we used a 2-step GIMO transfection protocol (Lin et al., 2011; Salman et al., 2015) and the transgenic p230p locus of the reporter *Pb* ANKA parasite line *Pb* ANKA-GFP-$Luc_{eef1\alpha}$ (676m1cl1) (parental). The fusion protein of GFP and firefly luciferase (LUC-IAV) is expressed under the constitutive *Pbeef1a* promoter. The reporter-cassette is integrated into the neutral *p230p* locus in chromosome 3. In the first step we deleted the *Pb csp* CDS and replaced it with the positive-negative selectable marker, to create a *Pb csp* deletion GIMO line (*Pb*ANKA-ΔCSP GIMO). In order to do this, we generated a construct (pL1929) that is based on the standard GIMO DNA construct pL0034. This construct contains the positive-negative (h*dhfr*::y*fcu)* selection marker (SM) cassette, and was used to insert both the *Pbcsp* 5' and 3' gene targeting regions (TR), encompassing the full length promoter and transcription terminator sequences, respectively, and was transfected into the parental *Pb* ANKA-GFP-$Luc_{eef1\alpha}$ parasites (676m1cl1) using standard methods of transfection (Janse et al., 2006). The following primers were used:

Primers for the DNA Constructs for the Generation of the Chimeric Parasite Line

DNA Construct	Primer No.	Primer sequences*	Restr. sites	Frag. size (bp)	Description
pL1972, pL1929	**1178**	cat**gggccc**TTAAGACATAAAAGGGAATA TGGAATATACTAGC	ApaI	1584	PbCSP 5'-UTR promoter sequence, F
	1179	at**ccgcgg**TAGCTAATTTTCTCATCATG AATTGGGATC	SacII		PbCSP 5'-UTR promoter sequence, R
	1180	at**cccggg**AGCTTTAATTAAATAAACAT TACGCATG	XmaI	939	PbCSP 3'-UTR sequence, F
	1181	ataagaat**gcggccgc**ATAATATATATTAGG AGAATTAACCAATGCTG	NotI		PbCSP 3'-UTR sequence, R
	1011	cccg**ctcgag**CGCCAATTCATGATGAG AAAATTAGC	XhoI	1235	PfCSP, F
	1012	ataagaat**gcggccgc**CTTTATCTAATTAA GGAACAAGAAGGATAATACC	NotI		PfCSP, R

Restr.: Restriction; Frag.: Fragment; No.: Number
*restriction site sequence are in bold and underlined

Transfected parasites were selected in mice by applying positive selection by providing pyrimethamine in the drinking water (Janse et al., 2006). Transfected parasites were cloned by limiting dilution (Salman et al., 2015), resulting in the *Pb*ANKA-ΔCSP GIMO line (line 2251cl1).

In the second step we replaced the positive-negative SM in the *Pb*ANKA-CSP GIMO genome with the *Pf csp* CDS by GIMO transfection to create the *Pb* chimeric CSP replacement line. This was achieved by modifying the construct used in the first step (pL1929);

specifically, the h*dfhr*::y*fcu* SM cassette was removed and replaced with *Pf csp* CDS sequence, generating plasmid pL1972. The *Pf csp* CDS was amplified from genomic DNA of the *Pf* NF54 strain. The pL1972 construct was sequenced to ensure there were no mutations in the *Pf csp* CDS using the primers listed above. The constructs were linearized using ApaI and NotI restriction enzymes outside of the 5' and 3' TRs before transfection. The construct was used to transfect parasites of the *Pb*ANKA-CSP GIMO line (line 2251cl1) using standard methods of GIMO-transfection (Lin et al., 2011). Transfected parasites were selected in mice by applying negative selection by providing 5-fluorocytosine (5-FC) in the drinking water of mice (Salman et al., 2015). Negative selection results in selection of chimeric parasites where the h*dhfr*::y*fcu* SM in the *csp* locus of *Pb*ANKA-CSP GIMO line is replaced by the CDS of *Pf csp*. Selected chimeric parasites were cloned by the method of limiting dilution. Correct integration of the constructs into the genome of chimeric parasites was analyzed by diagnostic PCR-analysis on gDNA and Southern analysis of pulsed field gel separated chromosomes as described elsewhere (Janse et al., 2006). Primers used for PCR genotyping are listed here:

Primers for Genotyping of the Chimeric Parasite Line

Primer No.	Description	Primer sequences *
1011	PfCSP F	cccg**ctcgag**CGCCAATTCATGATGAGAAAATTAGC
1012	PfCSP R	ataagaat**gcggccgc**CTTTATCTAATTAAGGAACAAGAAGGATAATACC
1042	Pb5'CSP promoter integration F	AGAGACAAACCAACCTTAGGAAC
1043	Pb5'CSP promoter integration R	CTTCCATAGCACTGGTATTCCTG
1044	Pb3'CSP UTR integration F	AGTTAGAATAAAGCCTGGCTCTG
1045	Pb3'CSP UTR integration R	TTACTATTCGTGCCCATTACGAC
1048	hDHFR-yFCU (+/-SM) F	ATCATGCAAGACTTTGAAAGTGAC
1049	hDHFR-yFCU (+/-SM) R	CATCGATTCACCAGCTCTGAC
1054	PbCSP F	CCAAAGGAACTTAAACGAGCTATG
1055	PbCSP R	CTTATACCAGAACCACATGTTACG

No.: Number

This method creates chimeric 'gene replacement' *Pb* parasites that lack the *Pb csp* CDS but express *Pf* CSP (*Pb*ANKA-*Pf*CSP(r)$_{PbCSP}$; line 2257cl2) (short: *Pb-PfCSP*) under the control of the *Pb csp* regulatory sequences.

*restriction site sequences are in bold and underlined

Mosquito Transgenesis

The transgenesis construct contained a reporter cassette with a gene encoding DsRed2 under the control of a nervous system-specific 3xPax3 promoter and SV40 terminator. The single-chain antibody (scFv) sequence was designed by linking the variable regions of the H- and L-chain of monoclonal antibody 125 by a glycine-rich linker (GGGGSGGGGSGGGGS). The *Anopheline* salivary gland-specific anti-platelet protein gene (*Aapp*) signal peptide was identified by SignalP 4.1 Server (http://www.cbs.dtu.dk/services/SignalP/) and Signal Blast programs (http://sigpep.services.came.sbg.ac.at/signalblast.html) and fused to the N-terminus of the scFv 125 sequence (sc125), whereas the Flag tag (DYKDDDDK) was fused to the C-terminus. The sequences were codon-optimized with the GENEius online tool using *A. gambiae* codon preference table (Volohonsky et al., 2015), synthesized and sequenced (Eurofins). The anti-CSP *scFv125* single-chain antibody gene was placed between the promoter of *Aapp* (AGAP009974) (Yoshida and Watanabe, 2006) and the SV40 terminator. Transgenes were assembled into *pDSAR* vectors and insertion into the XK docking line in the mosquito genome was mediated by φ*C31* integrase (Volohonsky et al., 2015). Because of the homozygous lethality of the insertion, each generation of dsRed2-positive *Aapp::125* heterozygous females was purified by COPAS sorting (Union Biometrica) and back-crossed with wild-type males (Ngousso strain). Expression of the transgene at transcript and protein level was confirmed by quantitative Real-Time-PCR and by immunoblotting using the anti-FLAG antibody, respectively (see also Supplemental Figures S3C and S3D).

In Vivo Plasmodium Infections

Female C57BL/6 mice were passively immunized (4-6 per group) by i.p. injection of 400 μg monoclonal antibody in 100 μl of PBS. One day later, *Pb-PfCSP* sporozoites ($5*10^3$) were injected s.c. into the mouse tail. For bite-back experiments, mice were exposed to the bites of wild-type or *Aapp::125* transgenic mosquitoes 18-19 days post *Pb-PfCSP* infection (range 1-9 infectious bites per mouse). Blood parasitaemia was assayed by daily tests of Giemsa-stained thin blood smears and a minimum of 100 microscopic fields were counted. After onset of parasitaemia, mice were monitored every 6-12 h for severe neurological and behavioral symptoms typical of experimental cerebral malaria (ECM) defined as hunched body position, grooming alteration, ataxia, paralysis, or convulsions (Lackner et al., 2006) or using the rapid neurological and behavioral test (RMCBS) (Carroll et al., 2010). Mice with ECM symptoms or with a RMCBS score $\leq$ 5 (out of 20) were sacrificed immediately.

Passive antibody transfer and challenge experiments with *PfGFP-luc* sporozoites using FRG-huHep mice were performed as previously published (Ishizuka et al., 2016) (Sack et al., 2017). Hepatocyte donor-matched mice were administered i.p 150 μg/mouse of monoclonal antibody in 200 μl of PBS the day before challenge. Mice were infected by exposing them to mosquitoes (n=50, 50% infection rate with an average of >10 oocysts/mosquito). Parasite liver burden was assessed as previously published (Ishizuka et al., 2016) using an IVIS imaging system and LivingImage software. To determine "% of control" parasite liver burden, the average total flux (photons/second) of all control mice was averaged and the "% of control" for each mouse was calculated as a percentage of this value. Results are expressed as a percentage of the average parasite liver burden of mice given control monoclonal antibody mGO53 (Wardemann et al., 2003).

Immunofluorescence Assay

Pf NF54, *Pb-PfCSP* or *Pb* parental salivary gland sporozoites ($4*10^4$/well) were air-dried overnight on 8-well microscopy slides (Medco) pre-coated with 3% BSA in RPMI. After fixation with 4% paraformaldehyde (PFA, Alfa Alsar), sporozoites were blocked with 10% FCS/PBS and then incubated for 45 min at 37 °C or 1-2 h at RT in duplicates with 20-25 μl of serum or monoclonal antibodies (100 μg/ml) diluted in 10% FCS/PBS. The monoclonal antibody 2A10 was used as a positive control for *Pf* (Zavala et al., 1983) and *Pb-PfCSP* and 3D11 (Yoshida et al., 1980) for *Pb* sporozoites. Bound antibodies were revealed by incubation for 45 min at 37 °C or 1h at RT with a Cy3-conjugated goat anti-human-IgG (diluted 1:1,000; Jackson Immuno Research) or an Alexa Fluor®488 goat anti-mouse IgG (diluted 1:1,000; Life Technologies), respectively. Images were acquired on an AxioObserver Z1 fluorescence microscope equipped with an Apotome module (Zeiss) using the 63x objective or a DMI-300B Leica fluorescence microscope. Images were analyzed using the AxioVision ZEN 2012 software (Zeiss) and ImageJ (Rasband, 1997-2015).

Sporozoite Hepatocyte Traversal Assay

Traversal assays were performed as described elsewhere (Behet et al., 2014). Briefly, $6*10^4$ cells/well of a human hepatocyte cell line (HC-04, MRA-975, deposited by Jetsumon Sattabongkot) were seeded into a 96-well plate (Greiner, TPP and Costar) and incubated for 24 h at 5% CO_2 and 37 °C (70% confluency). Isolated *Pf* salivary gland sporozoites (10^5) were pre-incubated with 100 μg/ml monoclonal antibodies in 50 μl for 30 min on ice. $5*10^4$ sporozoites per well were then seeded in duplicates onto HC-04 cells in presence of 0.5 mg/ml dextran-rhodamine (Molecular Probes) and a final antibody concentration of 50 μg/ml. As a negative control sporozoites pre-treated for 5 min on ice with the actin polymerization inhibitor Cytochalasin D (1.25 μg/ml, Sigma Aldrich) were used. Non-treated sporozoites were used as a positive control and non-infected cells incubated with dextran-rhodamine were used as background control. The plates were centrifuged for 10 min at 3,000 rpm at RT without brakes. After 2 h, cells were trypsinized and fixed in 1% PFA in PBS. Dextran-rhodamine positive cells were quantified by flow cytometry (LSR II, BD Biosciences). Sporozoite cell traversal rates were determined after correction for background dextran incorporation in non-infected cells. Sporozoite traversal of untreated sporozoites was set as 0% traversal inhibition.

Exoerythrocytic Forms Developmental Assay

HC-04 cells (10^4 /well) were seeded into a rat collagen (BD Biosciences) pre-treated 96-well plate with transparent bottom (Nalgene International). *Pb-PfCSP* salivary gland sporozoites (10^4) were pre-incubated for 30 min on ice with or without 50 μg/ml (antibody 125 in Extended Data Fig. 5e) or 100 μg/ml monoclonal antibodies. *Pb-PfCSP* sporozoites were then added to the cells in triplicates and the plate was centrifuged at 110xg for 1 min at RT. After 2 h of incubation extracellular sporozoites were removed by three washes with 2% combined penicillin and streptomycin solution with 5 μg/ml fungizone and one time without fungizone. Two days later, the cells were fixed with 4% PFA for 15 min at RT before permeabilization with 50 μM NH_4Cl_2 (Sigma Aldrich), 3% FBS, 0.3% Triton (Sigma Aldrich) for 1 h at 37 °C. Development of exoerythrocytic forms (EEFs) was examined using rabbit anti-GFP antibody (1:1,000; Abcam) diluted in permeabilization buffer for 1 h at 37 °C and AlexaFluor®555 conjugated anti-rabbit-IgG antibody (1:1,000; Molecular Probes). Nuclei were stained with DAPI (1.25 μg/ml, Molecular Probes). Images were acquired in the 96 well plates on an AxioObserver Z1 fluorescence microscope equipped with an Apotome module (Zeiss, 10x objective). EEF numbers were counted using the AxioVision ZEN 2012 software (Zeiss). EEF development of untreated sporozoites was set as 0% of EEF inhibition.

Quantitative Real-Time (RT)-PCR

Aapp::*125* transcripts were examined by quantitative RT-PCR in the thoracic and abdominal segments of the transgenic mosquitoes. Total RNA was extracted from thoraxes and abdomens of 15 mosquitoes with TriReagent (Sigma Aldrich) according to the manufacturer's protocol. Total RNA (2 μg) was converted into cDNA using the RevertAid H Minus Reverse Transcriptase kit (Fermentas) and random hexamers (Fermentas). Quantitative PCR reactions were run on a StepOnePlus™ RT-PCR instrument (Applied Biosystems) using the Fast SYBR® Green Master mix (Applied Biosystems) according to the manufacturer's protocol. Specific primers amplified a 66 nt fragment connecting the signal peptide and the scFv (VB739: 5'-*GAAGTTTCTACTGCTTGTGGCTAGTGT*-3' and VB740: 5'-*AGCTGGATCTGGGCGGATA*-3').

Immunoblotting

Transgenic *Aapp::125* mosquitoes were cut with micro-scissors (World Precision Instruments) along the abdomen-thorax junction. Thoraxes and abdomens of 15 mosquitoes were ground in 50 mM Tris HCl, 150 mM NaCl, 1% Triton, 0.1% SDS (Sigma Aldrich) in the

presence of 1x Protease Inhibitor Mix (Roche), incubated on ice for 10 min and centrifuged at maximal speed (13,200 rpm) for 15 min. Total protein extracts (25 μg) were separated on a 10% SDS-PAGE in reducing conditions and transferred to a nitrocellulose membrane (GE Healthcare), according to the manufacturer's protocol. Membranes were blocked with 5% milk (BioRad) and 0.1% Tween20 (Sigma Aldrich) in PBS and incubated with polyclonal anti-FLAG antibody (1:1,000; Sigma Aldrich). Polyclonal antibodies against blood born protein prophenoloxidase 2 (PPO2) (1:15,000) served as loading control (Fraiture et al., 2009). Goat anti-rabbit HRP-conjugated antibodies (Pierce, Thermo Scientific) were used at 1:10,000. Bound antibodies were detected by reaction with Pierce ECL Western Blotting Substrate (Pierce, Thermo Scientific).

Fab Production

V_K and V_H regions were cloned into expression vectors upstream of human Igκ and Igγ1 constant regions, respectively, as previously described (Tiller et al., 2008). IgG were transiently expressed in HEK 293F cells and purified via Protein A affinity chromatography (GE Healthcare). Fabs were generated by papain digestion, and purified via an additional Protein A chromatography step, followed by cation exchange chromatography (MonoS, GE Healthcare), and size exclusion chromatography (Superdex 200 Increase 10/300 GL, GE Healthcare).

CSP Production

CSP full length (7G8 strain) was cloned into pHLsec for transient expression in HEK293 cells. CSP was purified via HisTrap Ni-NTA (GE Healthcare) and size exclusion chromatography (Superdex 200 Increase 10/300 GL, GE Healthcare) prior to binding studies.

Germline Reversion

Germline genes of cluster 2 (580) and cluster 4 (663) were designed using the predicted germline V(D)J gene segments of the H- and L-chain of the respective antibody according to IgBLAST and IMGT. The addition of random N-nucleotides in the CDR3 region of the H-chain during somatic recombination does not allow reversion of this region of the H-chain.

Alignment of nucleotide and amino acid sequences of the HCDR3 and KCDR3 for Cluster 2 and their inferred germline sequence.

Antibody	aa HCDR3	nt HCDR3
Cluster 4		
436	DPGGDSSPAGRTWFDP	GATCCGGGAGGAGATAGCAGCCCCGCGGGGGAGAACCTGGTTCGACCCC
580	DPGGDSSPAGRTWFDP	GATCCGGGAGGAGATAGTAGTCCCGCGGGGAGAACCTGGTTCGACCCC
674	DPGGDSSPAGRTWFDP	GATCCGGGAGGAGATAGCAGCCCCGCGGGGAGAACCTGGTTCGACCCC
678	DPGGDSSPAGRTWFDP	GATCCGGGAGGAGATAGCAGCCCCGCGGGGAGAACCTGGTTCGACCCC
germline	DPGGDSSPAGRTWFDP	GATCCGGGAGGAGATAGTAGTCCCGCGGGGAGAACCTGGTTCGACCCC
Cluster 2		
007	LLIFENDVGIDF	CTTCTTATATTTGAGAATGATGTGGGGATAGACTTC
350	LLILDSSEGVDF	CTTCTTATCTTAGACAGTAGTGAGGGGGTAGACTTC
349	LLILESDVGVDF	CTTCTCATATTAGAGAGTGATGTGGGGGTAGACTTC
125	LLILESDVGVDF	CTTCTTATATTGGAGAGTGATGTGGGGGTAGACTTC
316	LLILETDMGVDF	CTTCTTATATTAGAGACTGATATGGGGGTAGACTTC
191	LLIYESDVGVDF	CTTCTTATATATGAGAGTGATGTGGGAGTAGACTTC
663	LLIYESDVGVDF	CTTCTTATATATGAGAGTGATGTGGGAGTAGACTTC
germline	LLILESDVGVDY	CTTCTTATATTGGAGAGTGATGTGGGGGTAGACTAC
Antibody	aa KCDR3	nt KCDR3
Cluster 4		
436	QQYYSSPIT	CAGCAATATTATAGTAGTCCGATCACC
580	QQYYSSPIT	CAGCAATATTATAGTAGTCCGATCACC
674	QQYYSTPIT	CAACAATATTATAGTACTCCGATCACC
678	QQYYSSPIT	CAGCAATATTATAGTAGCCCGATCACC
germline	QQYYSTPIT	CAGCAATATTATAGTACTCCTATCACC
Cluster 2		
007	VQTVQAPYA	GTACAAACTGTGCAAGCTCCGTACGCT
350	LQTVQAPYS	CTCCAAACTGTGCAAGCTCCTTACAGT
349	VQTVQAPYT	GTGCAAACTGTACAAGCTCCCTACACT
125	VQTVNTPYA	GTGCAAACTGTAAATACTCCGTATGCA

(*Continued on next page*)

Continued

Antibody	aa KCDR3	nt KCDR3
316	VQTVQVPYT	GTGCAAACTGTACAAGTTCCGTACACT
191	VQTVQVPYT	GTGCAAACTGTACAAGTTCCGTACACT
663	VQTVQVPYT	GTGCAAACTGTACAAGTTCCGTACACT
germline	MQALQTPYT	ATGCAAGCTCTACAAACTCCCTACACT

aa: amino acid; HCDR3: H-chain complementarity determining region 3; nt: nucleotide; KCDR3: kappa chain complementarity determining region 3
CDR3 regions of the H-chain were thus inferred from the most commonly used residue at each position of the CDR3 regions of all clonally related cluster members of the respective antibody. CDR3 regions of the L-chain were reverted to complete germline.

Biolayer Interferometry Binding Studies

BLI (Octet RED96, ForteBio) experiments were conducted to determine the specificity and binding kinetics of 580-g-Fab, 580-Fab, 663-g-Fab and 663-Fab for *Pf* CSP (7G8 strain). *Pf* CSP was diluted to 10 μg/ml in kinetics buffer (PBS, pH 7.4, 0.01% (w/v) BSA, 0.002% Tween20) and immobilized onto Ni-NTA (NTA) biosensors (FortéBio). Following establishment of a stable baseline with loaded ligand in kinetics buffer, biosensors were dipped into wells containing 2-fold dilution series of Fab. Tips were then dipped back into kinetics buffer to monitor the dissociation rate. Kinetics data were analyzed using FortéBio's Data Analysis software 9.0, and curves were fitted to a 1:1 binding model.

Crystallization and Structure Determination

Purified 580-g-Fab and 663-Fab were concentrated to 12 mg/ml and diluted to 10 mg/ml with $NANP_5$ (10 mg/ml) in a 1:5 molar ratio prior to crystallization trials. Crystals for 580-g-Fab-$NANP_5$ grew in 10% (v/v) isopropanol, 100 mM HEPES pH 7.5, 20% (w/v) PEG 4000 and were cryoprotected in 10% (w/v) glycerol. Crystals for 663-Fab-$NANP_5$ grew in 100 mM tri-sodium citrate pH 5.5, 20% (w/v) PEG 3000 and were cryoprotected in 15% (w/v) glycerol. 580-Fab, 663-g-Fab and 663-Fab were crystallized in their unliganded forms. Crystals of 580-Fab grew in 100 mM MES pH 5, 1.6 M $(NH_4)_2SO_4$ and were cryoprotected in 20% (w/v) glycerol. Crystals of 663-g-Fab grew in 100 mM Tris pH 8.5, 200 mM $MgCl_2$, 20% (w/v) PEG 4000 and were cryoprotected in 10% (w/v) glycerol. Crystals of 663-Fab grew in 200 mM di-ammonium hydrogen citrate, 20% (w/v) PEG 3350 and were cryoprotected in 15% (w/v) glycerol. Data were collected at the 08ID-1 beamline at the Canadian Light Source (CLS), processed and scaled using XDS (Kabsch, 2010). The structures were determined by molecular replacement using Phaser (McCoy et al., 2007). Refinement of the structures was carried out using phenix.refine (Adams et al., 2010) and iterations of refinement using Coot (Emsley et al., 2010). All software was accessed through SBGrid (Morin et al., 2013).

SAXS Data Collection and Processing

SAXS data were collected at the BioSAXS 18-ID-D beamline at the Argonne Photon Source. 580-Fab and 663-Fab were co-complexed with *Pf* CSP (7G8 strain) in a 1.7:1 molar ratio of Fab to *Pf* CSP. Data on *Pf* CSP alone was also collected. Samples were applied to an in-line SEC-SAXS instrument at a flow rate of 0.7 ml/min, and images were collected after 1s exposure. Buffer control samples were derived from regions in the SEC-SAXS profile preceding elution of the sample and were used to correct the scattering curves. Approximately 10 frames from the SEC peak were averaged to generate an idealized scattering curve using PRIMUS (Figure S5A) (Konarev et al., 2003). The Kratky and Guinier plots were inspected to assess the presence of unfolding, aggregation or radiation damage (Figure S5C). The radius of gyration was determined from the Guinier plot using AutoRg (Konarev et al., 2003). The distance distribution function P(r) was obtained by indirect Fourier transform, which generated an estimate of the D_{max} and the Porod volume (Figure S5D). The apparent molecular weight was estimated by dividing the Porod volume by 1.7. Twenty *ab initio* models were generated using DAMMIF (Franke and Svergun, 2009) and averaged using DAMAVER (Volkov and Svergun, 2003). Chimera was used to visualize and dock the atomic structures into the SAXS envelopes.

Surface Plasmon Resonance

SPR measurements were performed with a BIACORE T200 (GE Healthcare) instrument docked with a series S sensor chip CM5 (GE Healthcare). Anti-human IgG antibodies in 10 mM HEPES with 150 mM NaCl at pH 7.4 (running buffer) were immobilized by amine-coupling using a human antibody capture kit (GE Healthcare) following the manufacturer's protocol. Equal concentrations of the sample and control antibody mGO53 (Wardemann et al., 2003) were captured in the sample and reference flow cell, respectively. After stabilizing the flow cells with running buffer at 10 μl/min flow rate for 20 min, $NANP_5$ dissolved in running buffer was injected at different concentrations: 0, 0.015, 0.09, 0.55, 3.3 and 20 μM. Maintaining the flow rate of 30 μl/min allowed the association and dissociation of $NANP_5$ for 60s and 180s, respectively, at 25 °C. Regeneration of both flow cells with 3 M $MgCl_2$ was conducted after each run. The data were fit using a 1:1 binding model or steady state kinetic analysis using the BIACORE T200 softwareV2.0.

QUANTIFICATION AND STATISTICAL ANALYSIS

Statistics were performed using R version 0.99.484 and GraphPad Prism 6.07. Normality of distribution was tested for all quantitative data sets by the Shapiro-Wilk test. Parametric or non-parametric tests were applied accordingly and are stated in the figure legends.

P values < 0.05 were considered significant (****: $p<0.0001$, **: $p<0.001$) and indicated in the figures. Mantel-Cox test was used for comparison of mice survival. Plots were produced using GraphPad Prism 6.07, Adobe Illustrator CS6 v16.0.3, ImageJ (Rasband, 1997-2015) and R version 0.99.484 using the ggplot2 package (R Development Core Team, 2008).

DATA AND SOFTWARE AVAILABILITY

The data that support the findings of this report are available from the corresponding authors upon reasonable request.

The crystal structures reported in this manuscript have been deposited in the Protein Data Bank, www.rcsb.org (PDB ID codes 6AZM, 5BK0, 5BK3, 5BK5 and 6AZX).